iScience

Article

Pharmaceutical inhibition of the Chk2 kinase mitigates cone photoreceptor degeneration in an iPSC model of Bardet-Biedl syndrome

Graphical abstract

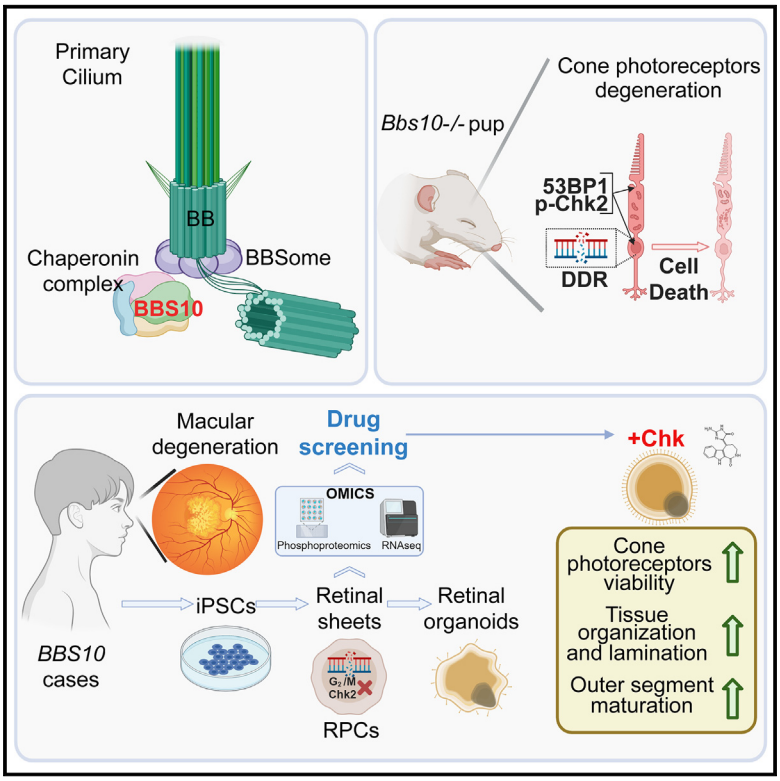

Highlights

- Bardet-Biedl syndrome is associated with photoreceptor degeneration
- Immature photoreceptors from *Bbs10*$^{-/-}$ pups present a DNA damage response
- Retinal progenitors and cones from *BBS10* iPSCs also present a DNA damage response
- Inhibition of the Chk2 kinase mitigates degeneration of cones from *BBS10* iPSCs

Authors

Andrea Barabino, Alisar Katbe, Roy Hanna, Benjamin S. Freedman, Gilbert Bernier

Correspondence

gbernier.hmr@ssss.gouv.qc.ca

In brief

Natural sciences; Biological sciences; Cell biology; Stem cells research;

Barabino et al., 2025, iScience *28*, 112130
April 18, 2025 © 2025 The Author(s). Published by Elsevier Inc.
https://doi.org/10.1016/j.isci.2025.112130

CellPress

iScience

CellPress
OPEN ACCESS

Article

Pharmaceutical inhibition of the Chk2 kinase mitigates cone photoreceptor degeneration in an iPSC model of Bardet-Biedl syndrome

Andrea Barabino,[1] Alisar Katbe,[1] Roy Hanna,[1] Benjamin S. Freedman,[2] and Gilbert Bernier[1,3,4,*]

[1]Stem Cell and Developmental Biology Laboratory, Hôpital Maisonneuve-Rosemont, 5415 Boul. L'Assomption, Montréal, QC H1T 2M4, Canada

[2]Division of Nephrology, Department of Medicine, Kidney Research Institute, and Institute for Stem Cell and Regenerative Medicine, University of Washington, Seattle, WA 98109, USA

[3]Faculty of Medicine, Department of Neurosciences, University of Montreal, 2960 de la Tour Road, Suite 111, Montreal, Quebec H3T 1J4, Canada

[4]Lead contact

*Correspondence: gbernier.hmr@ssss.gouv.qc.ca

https://doi.org/10.1016/j.isci.2025.112130

SUMMARY

Bardet-Biedl syndrome (BBS) is a syndromic ciliopathy leading to progressive blindness starting in childhood, but the mechanism of photoreceptor degeneration remains unclear. The basal body of the photoreceptor primary cilium originates from the centrosome's mother centriole, and BBS-related proteins form a complex at basal body. Centrosomes also organize microtubules of the mitotic spindle. We show here that photoreceptors from *Bbs10*$^{-/-}$ mouse pups present a DNA damage response (DDR) that becomes persistent and localizes to the basal body. In patient-derived induced pluripotent stem cells (iPSCs) carrying *BBS10* mutations, BBS retinal progenitor cells (RPCs) present a DDR that correlates with activation of the mitotic spindle checkpoint. Pharmaceutical inhibition of the Chk2 kinase in BBS RPCs mitigates cell death and genomic instability and restores the phospho-proteome. Drug treatment of BBS retinal organoids improves tissue organization, cone survival, and outer segment maturation, thus opening a possible therapeutic avenue to delay photoreceptor degeneration in BBS.

INTRODUCTION

Ciliopathies are a heterogeneous group of genetic diseases caused by aberrations in cilia assembly, maintenance, structure, and function.[1–4] Syndromic ciliopathies are multi-systemic, as cilia are found in almost all cells. They include Bardet-Biedl syndrome (BBS), Meckel-Gruber syndrome, Joubert syndrome, and nephronophthisis.[1] BBS is among the most severe ciliopathies that are compatible with life. The disorder is associated with obesity, kidney disease, cardiovascular and skeletal abnormalities, craniofacial and dental deformations, polydactyly, and degeneration of rod and cone photoreceptors.[5,6] Autosomal recessive mutations in *BBS10* account for nearly 40% of cases.[7] *BBS10* patients present rod-cone dystrophy, cone-rod dystrophy, or pure cone dystrophy starting during childhood.[8,9]

Photoreceptors are sensory neurons that generate electrical responses when stimulated by light. Rod photoreceptors are sensitive to dim light and involved in peripheral and night vision. Cone photoreceptors are sensitive to strong light and involved in central and day-light color vision.[10] The photoreceptors' primary cilium is a modified and unique type of sensory cilium and has an intracellular location.[11–13] Its outermost part is the outer segment (OS) that contains membranous discs arranged in a coin-stack like configuration, that accommodate the visual pigment densely packed within the disc lamellae. The connecting cilium (CC) is the site of high flow of lipids and proteins from their site of synthesis to the OS. The CC is essential in photoreceptor physiology and its dysfunction contributes to retinal degeneration.[11,14] The BBsome core complex is composed of the BBS1, BBS2, BBS4, BBS5, BBS7, BBS8/TTC8, BBS9, and BBS18/BBIP1 proteins, which form an octameric complex that localizes to the basal body of the primary cilium.[15–18] The BBsome complex constitutes a critical protein assembly essential for primary cilia function and maintenance. It is involved in key cellular processes, such as homeostasis, intraflagellar transport, and the translocation of molecular cargo via ciliary pathways. The complex also facilitates the interaction of cargo with kinesin motor proteins for transport mechanisms within cilia. BBS6, BBS10, and BBS12, while associated with the BBsome, are not components of its core structure. Instead, they form a chaperonin-like complex with CCT/TRiC, which is vital for the assembly and stability of the BBsome.[15,19,20] This complex ensures the correct folding and functionality of the BBsome proteins, which is required for the effective performance of its roles in ciliary transport and signaling. Accumulation of OS proteins in the cytoplasm of photoreceptors, or ectopic accumulation of non-OS proteins

This is an open access article under the CC BY-NC license (http://creativecommons.org/licenses/by-nc/4.0/).

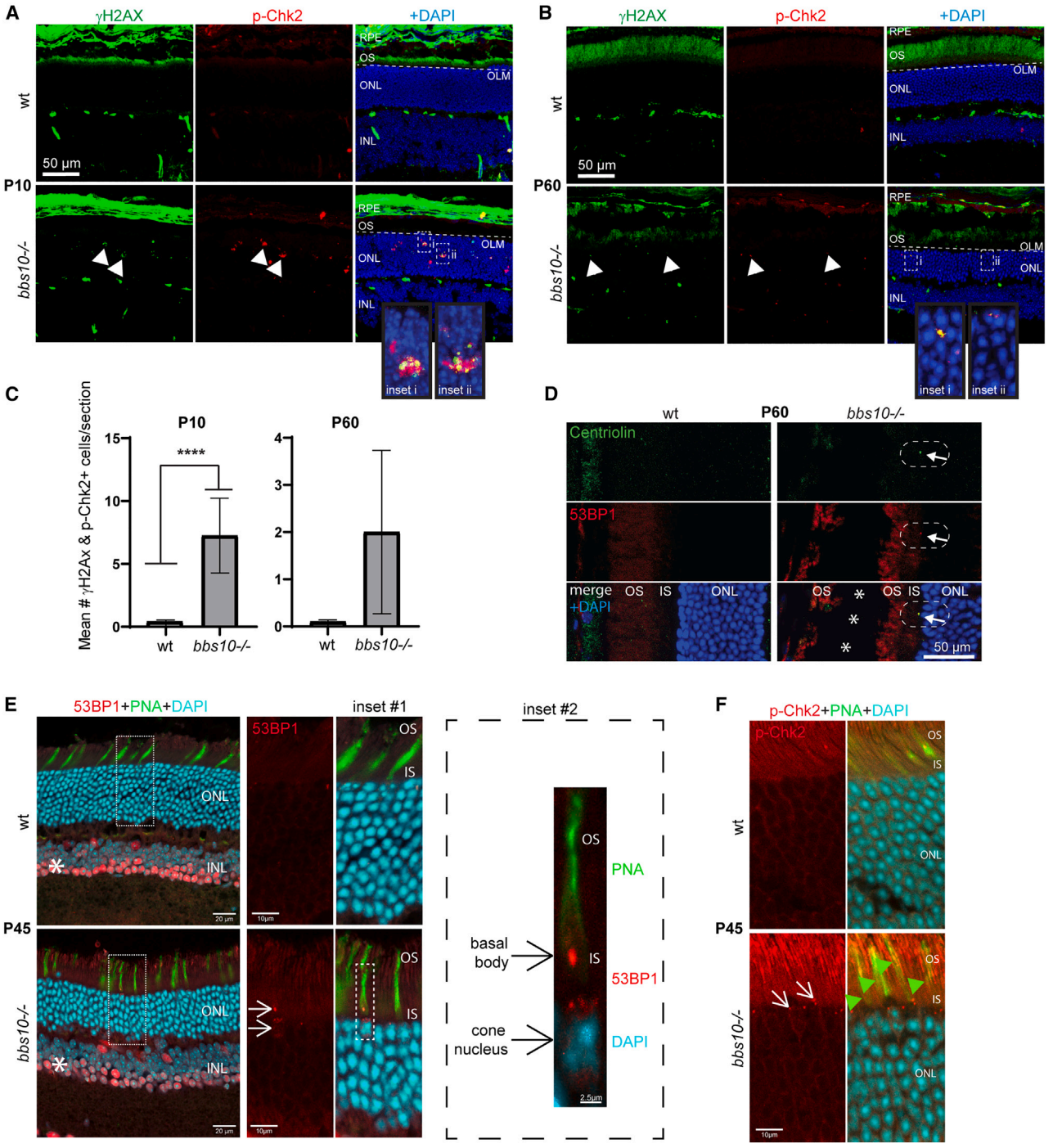

Figure 1. DDR activation in *Bbs10*$^{-/-}$ cone photoreceptors

(A) Representative confocal immunofluorescence images of wt and *Bbs10*$^{-/-}$ retinal sections at P10. Note accumulation of γH2AX and p-Chk2 foci in the outer nuclear layer (onl) of *Bbs10*$^{-/-}$ retinas (white arrows). Inner nuclear layer (inl), outer segment (os), retinal pigment epithelium (rpe), and outer limiting membrane (olm). Scale bar: 50 μm.

(B) Representative confocal immunofluorescence images of wt and *Bbs10*$^{-/-}$ retinal sections at P60. Note accumulation of γH2AX and p-Chk2 foci in the outer nuclear layer (onl) of *bbs10*−/− retinas (white arrows). Inner nuclear layer (inl), outer segment (os), retinal pigment epithelium (rpe), and outer limiting membrane (olm). Scale bar: 50 μm.

(C) Quantification of results presented in (A) and (B) as the sum of all γH2AX and p-Chk2 foci. $n = 5$ retinal sections/sample, with 2 biological replicates. All values are mean ± SEM.

(****) $p < 0.0001$ by Student's unpaired t test.

(legend continued on next page)

in the OS, such as observed in various *bbs*-null mouse models, is thought to be the main mechanism of cell death.[21–24]

Cilia are present in most cell types but were traditionally described in epithelial cells. The ciliary axoneme is anchored and develops from a specialized centriole called the basal body (BB) that operates as a microtubule-organizing center.[25] The BB is composed of a symmetric and radial arrangement of nine triplets of microtubules, whence the external doublet of microtubules of the axoneme extends. The axoneme is a microtubule structure formed by aligned alpha and beta-tubulin arranged in a radial array of 9 doublets.[25] Primary cilia can be distinguished from motile cilia for the absence of a central pair of microtubules. While motile cilia have a "9 + 2" structure, non-motile primary cilia lack this central pair, so define as a "9 + 0" structure.[2,4,26] Cilia are generally formed in the G0 or G1 phase of the cell cycle but can also be observed during S/G2 phase. Cilium formation is restricted to these phases because the BB, which is derived from the mother centriole of the centrosome, is essential for mitotic spindle formation and function during cell division.[27–30] For this reason, before cells enter mitosis, the primary cilium is disassembled to release the centrioles. After cytokinesis, when the mitotic process is complete, and the cell re-enters the G0 phase, ciliogenesis restarts. Upon detection of damage or genomic instability in M phase, the spindle assembly checkpoint (SAC) prevents completion of mitosis, allowing time for damage repair or alternatively, triggering programmed cell death.[31,32] Key sensors and mediators of this process are the DNA damage response (DDR) proteins ATM, ATR, Chk1, and Chk2.[33,34]

BBS10 is part of the TCP-1 chaperonin family and structural analysis predicts that it is a probable chaperonin. However, the BBS10 protein is not part of the BBsome, and BBS10 molecular function remains poorly characterized.[19,20] Importantly, the mechanism of photoreceptor cell death and disease selectivity in BBS is unclear, and no treatment exists to prevent patient's blindness. Using directed differentiation of induced pluripotent stem cells (iPSCs) carrying *BBS10* mutations into retinal sheets, we previously reported that BBS retinal precursors show multiple developmental anomalies together with transcriptomic SAC activation and genomic instability.[35,36] They also show upregulation of genes related to neural/retinal development (DLX1, VSX1, and SIX6), differentiation (NEUROD4 and ASCL1/MASH1), and function (SLC32A1 and NTRK1).[35] We report here that DDR proteins accumulate in immature photoreceptors from *Bbs10*$^{-/-}$ mice, and that 53BP1 and p-Chk2 show persistent localization at the BB of the primary cilium in surviving cones. RNA-sequencing (RNA-seq) analysis of BBS retinal progenitor cells (RPCs) confirmed SAC activation. Treatment of BBS RPCs with Chk2 or ATM inhibitors blocks the DDR, promotes cell survival, and restores the abnormal phospho-proteome. Prolonged treatment of BBS retinal organoids with a Chk2 inhibitor (C2i) improves retinal tissue organization, mitigates the DDR, and promotes cone photoreceptor survival and OS maturation.

RESULTS

Early-onset DDR in *Bbs10*$^{-/-}$ mouse's photoreceptors

Bbs10$^{-/-}$ mice were reported to display photoreceptor degeneration and reduced visual function at least from postnatal day 19 (P19), with a complete absence of cone electroretinogram (ERG) and reduced rod ERG at P30.[21] To validate these finding and test for genomic instability, we performed histological analyses of wild type (wt) and *Bbs10*$^{-/-}$ mice at P10 and P60 to determine the kinetics of cone degeneration. In mice, all cones and rods are already post-mitotic at P10.[37] We observed that the number of M-opsin-positive inner/outer segments was comparable between wt and *Bbs10*$^{-/-}$ mice at P10 but highly reduced in *Bbs10*$^{-/-}$ mice at P60 (Figures S1A–S1C), suggesting that cones are produced in normal number. We observed that M-opsin was not entirely distributed in the OS of cones in *Bbs10*$^{-/-}$ mice but also present around the nucleus and at the endfeet of photoreceptors. Similar localization anomalies were observed looking at acetylated alpha tubulin, suggesting defective protein transport (Figures S1A and S1B, yellow and green arrows). Using the TUNEL assay, photoreceptor cell death was readily detectable and more frequent at P10 than at P60 in *Bbs10*$^{-/-}$ mice, with notable reduction of the photoreceptor outer nuclear layer (ONL) thickness at P60 (Figures S1A–S1C). DDR kinases, such as ATM, ATR, Chk1, and Chk2 can phosphorylate p53 to induce cell-cycle arrest and/or apoptosis.[38] We investigated this as a possible alternative mechanism to explain photoreceptor cell death in BBS. Notable accumulation of p-Chk2 and of the histone variant γH2AX (a marker of DNA double-strand breaks) was observed in the cell' nucleus throughout the photoreceptor ONL of *Bbs10*$^{-/-}$ mice at P10 (Figures 1A and 1C).[39] At P60, the number of DDR-positive cells in the ONL was much lower and positive cells were generally, but not exclusively, located near the outer limiting membrane (Figures 1B and 1C). Because DDR foci at P60 localized both inside and outside the DAPI-positive nuclei, we investigate possible localization at the BB of photoreceptors. Hence, we observed rare 53BP1-positive foci co-localizing with centriolin at P60 (Figure 1D). Between P4 and P11, mouse cone's nuclei are not located near the outer limiting membrane but rather dispersed in the ONL, precluding distinction between cones and rods.[40] To distinguish between these, we used mice at an intermediate age, thus before cone depletion

(D) Confocal immunofluorescence of wt and *Bbs10*$^{-/-}$ retinal sections at P60, revealing rare 53BP1 foci that show co-localization with centriolin (white arrow). Outer segment (os), inner segment (is), and outer nuclear layer (onl). Scale bar: 50 μm. Asterix indicate an histological artifact in the retinal section of *Bbs10*$^{-/-}$ mice.

(E) Confocal immunofluorescence of wt and *Bbs10*$^{-/-}$ retinal sections at P45. Note the 53BP1 foci in PNA-positive cones of *Bbs10*$^{-/-}$ retinas (white arrows in inset #1). 53BP1 foci in *Bbs10*$^{-/-}$ cones localized to the basal body and around the nucleus (black arrows in inset #2). 53BP1 labeling of nuclei of the inner nuclear layer (inl) is unspecific (asterix). Outer nuclear layer (onl), inner segment (is), and outer segment (os). Scale bars: 20 μm and 10 μm, respectively.

(F) Confocal immunofluorescence of wt and *Bbs10*$^{-/-}$ retinal sections at P45. Note the p-Chk2 foci in PNA-positive cones of *bbs10*−/− retinas and which localized to the basal body (white arrows). A robust p-Chk2 signal is also observed in the photoreceptor outer segments. The PNA positive cone outer segment is indicated (green arrows). Inner nuclear layer (inl), outer nuclear layer (onl), outer segment (os). Scale bars: 20 μm and 10 μm, respectively.

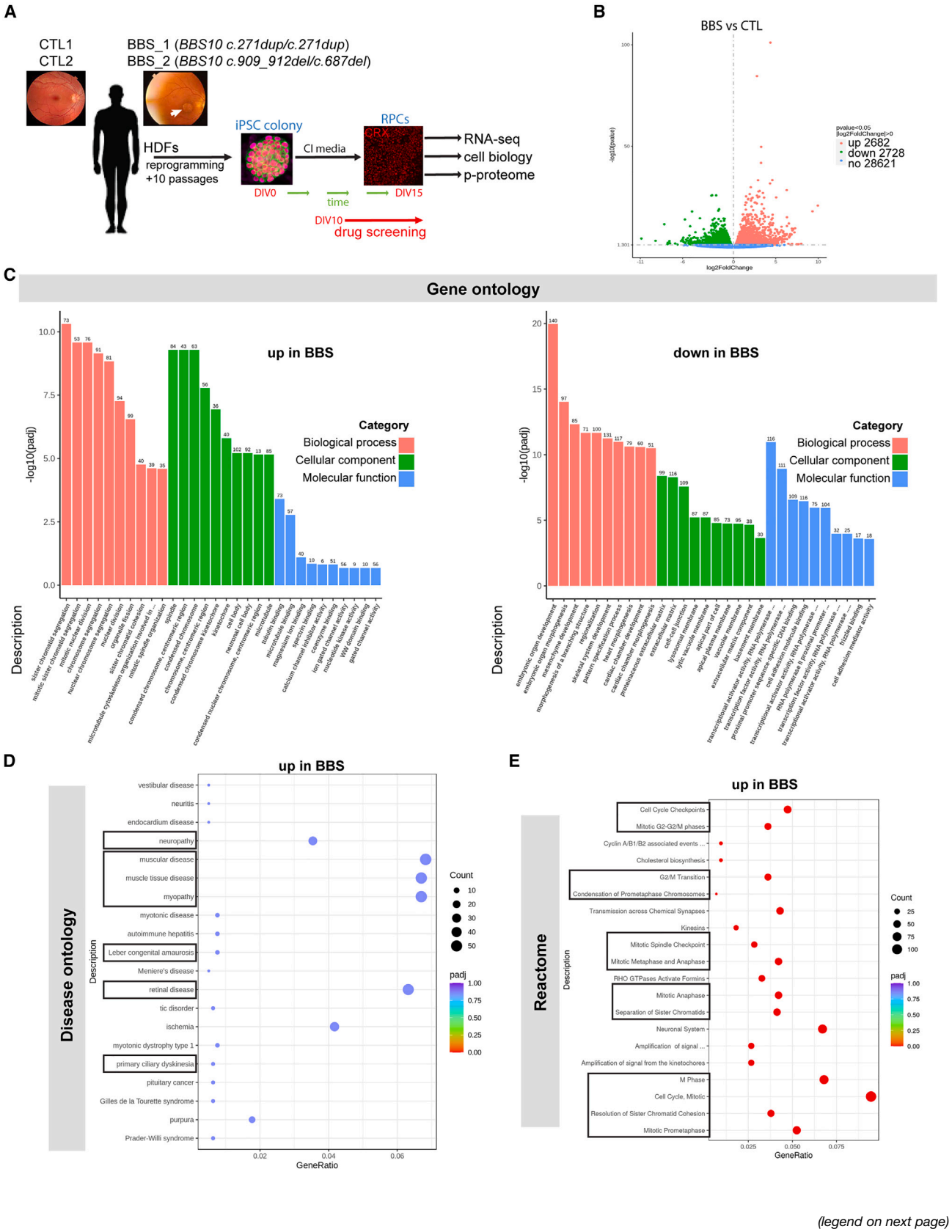

(legend on next page)

but when the OS is formed. Using the peanut agglutinin (PNA) lectin, which labels the cone OS, we observed accumulation of 53BP1 (a generic DDR protein) and p-Chk2 foci in PNA-positive cones of *Bbs10*$^{-/-}$ mice at P45 (Figures 1D and 1E).[41,42] Accumulation of DDR proteins was not observed in the other nuclei of the ONL, presumably rods. In cones, 53BP1 and p-Chk2 were generally localized at the apex of the cone cell body (Figures 1D and 1E) and near the BB of the primary cilium (Figure 1D-inset). Diffuse 53BP1 signal was also observed around the nucleus (Figure 1D-inset). Notably, mitotic 53BP1 localizes to the centrosome and spindle pole, and 53BP1 depletion induces mitotic defects.[43] This suggested that photoreceptor cell death in *Bbs10*$^{-/-}$ mice may be link to early activation of the DDR, which persists in both the nucleus and BB of remaining photoreceptors.

Activation of the spindle assembly checkpoint in BBS RPCs

Using iPSC lines from 2 independent controls (CTL) and 2 independent BBS cases with *BBS10* mutations (see STAR Methods), we generated day *in vitro* 15 (DIV15) RPCs using COCO/DAND5, which biases human pluripotent stem cell differentiation toward cone cell fate at the expanse of rods (Figure 2A).[35,36] At DIV5, COCO-induced RPCs show high SOX2 levels. At DIV10–DIV15, SOX2 is downregulated, with high RAX and low CHX10 and CRX levels. At DIV21, CRX is up-regulated, together with S-opsin.[36] In mice, *Crx* expression starts at embryonic day 12.5 in cone precursors, and strong expression is observed later in photoreceptors and subsets of bipolar neurons.[44] In human embryos, earliest *CRX* expression was reported at day 57.[45] CRX was also detected by immunofluorescence at day 70 (week 10) throughout the retina's outer neuroblastic layer, co-expressing CHX10 and the mitotic marker MIB-1.[46] While early and late RPCs are though not to express CRX, scRNA-seq analysis revealed the presence of a proliferating cone photoreceptor cluster in day 54, 56, and 70 human embryonic retinas.[47,48] Thus, proliferating intermediate retinal progenitors may exist between true RPCs and T1-T3 precursors. For simplicity however, we herein refer to the DIV15 cell population as RPCs, although it likely contains mixed populations of RPCs, retinal precursors, and non-retinal cells. Using DIV15 RPCs, we performed RNA-seq, cell biology and phospho-proteome analyses together with a small-scale drug screening (Figure 2A). RNA-seq analysis of differentially expressed genes (DEGs) between CTL and BBS revealed 2,682 up-regulated and 2,728 downregulated in BBS samples (Figure 2B). Heatmap analysis showed significant perturbation of cilia-related and actin filament bundle assembly genes in BBS RPCs, including downregulation of CCDC-related genes, involved in dynein-mediated cargo transport along the primary cilium, as well as KIF17, CFAP251, CFAP91, and DNAI family members, involved in dynein and kinesin-mediated axonemal transport and/or microtubule binding (Figures S2A and S2B). KIAA1009 (CEP162) and RPGRIP1L (NPHP8), both components of the transition zone (TZ) beneath the basal body, were among the most up-regulated cilia-related genes in BBS RPCs.[49,50] Notable up-regulation of GLI1 and GLI2, effectors of the Sonic Hedgehog signaling pathway, which is organized by cilia, was also observed in BBS samples (Figure S2A).[51] Gene ontology analysis revealed that sister chromatin segregation, chromosome segregation, and spindle were the most significant up-regulated pathways in BBS RPCs (Figure 2C). Most downregulated pathways were related to embryonic organ development/morphogenesis, extracellular matrix, and RNA Pol2 activity (Figure 2C). Disease ontology analysis showed that neuropathy, myopathy, retinal disease, and primary ciliary dyskinesia were the most relevant pathways in BBS samples (Figure 2D). Reactome analysis confirmed that mitotic spindle checkpoint and mitotic prometaphase, metaphase, and anaphase-related pathways were strongly activated in BBS, suggesting stalling of the mitotic phase in BBS RPCs (Figure 2E). Taken as a whole, these results were consistent with the known developmental and ciliary defects in BBS and suggested that SAC activation is central to the retinal degenerative process in BBS.

Chk2 inhibition improves cell viability and genomic stability in BBS RPCs

In response to DNA damage or genomic instability, the ATM/Chk2/p53 pathway arrests the cell cycle. ATM also localizes "by default" to the centrosome to monitor mitotic spindle integrity.[52–55] Activated ATM can phosphorylate Chk2, leading to mitotic arrest.[38] HSP90 is the most important chaperone, and response to protein misfolding was previously reported in *BBS10* models.[35] To test for molecules that could improve survival of BBS RPCs, we exposed or did not expose DIV10 CTL and BBS retinal progenitors to DMSO, or incremental concentrations of p53 (Pifithrin), Chk2 (Chk2i and Chk2iII), or HSP90 (Monorden) inhibitors for 5 days (Figure S3A). In this pilot assay, Pifithrin did not show positive effects at low concentration and was toxic at higher concentration and thus was excluded. HSP90i could reduce cell death, p-Chk2 and γH2AX accumulation in BBS RPCs (Figures S3B–S3D), with many cells however resembling senescent cells i.e., flat cells with a very large cytoplasm (Figure S3C). While both Chk2 inhibitors provided improvement, C2i was the most efficient (Figures S3B–S3D). To confirm this, we performed two additional independent

Figure 2. Sister chromatid segregation anomalies and activation of the mitotic spindle checkpoint in BBS RPCs

(A) Schematic of the experimental setup. CTL and BBS iPSCs were differentiated in CI media for 10 days and exposed or not to drugs for 5 days. RPCs (expressing low CRX) were subjected to RNA-seq, cell biology and phospho-proteome analyses at DIV15.

(B) Volcano plot from RNA-seq analysis of DIV15 CTL (n = 4) and *BBS* (n = 4) RPCs. Up and down regulated genes in BBS are showed. n = 2 biological replicate/sample, N total = 8.

(C) Gene ontology analysis of CTL and BBS RPCs at DIV15, showing pathways up and down in BBS. Biological process (BP), cellular context (CC), and molecular function (MF).

(D) Disease ontology analysis of CTL and BBS RPCs at DIV15.

(E) Reactome analysis of CTL and BBS RPCs at DIV15.

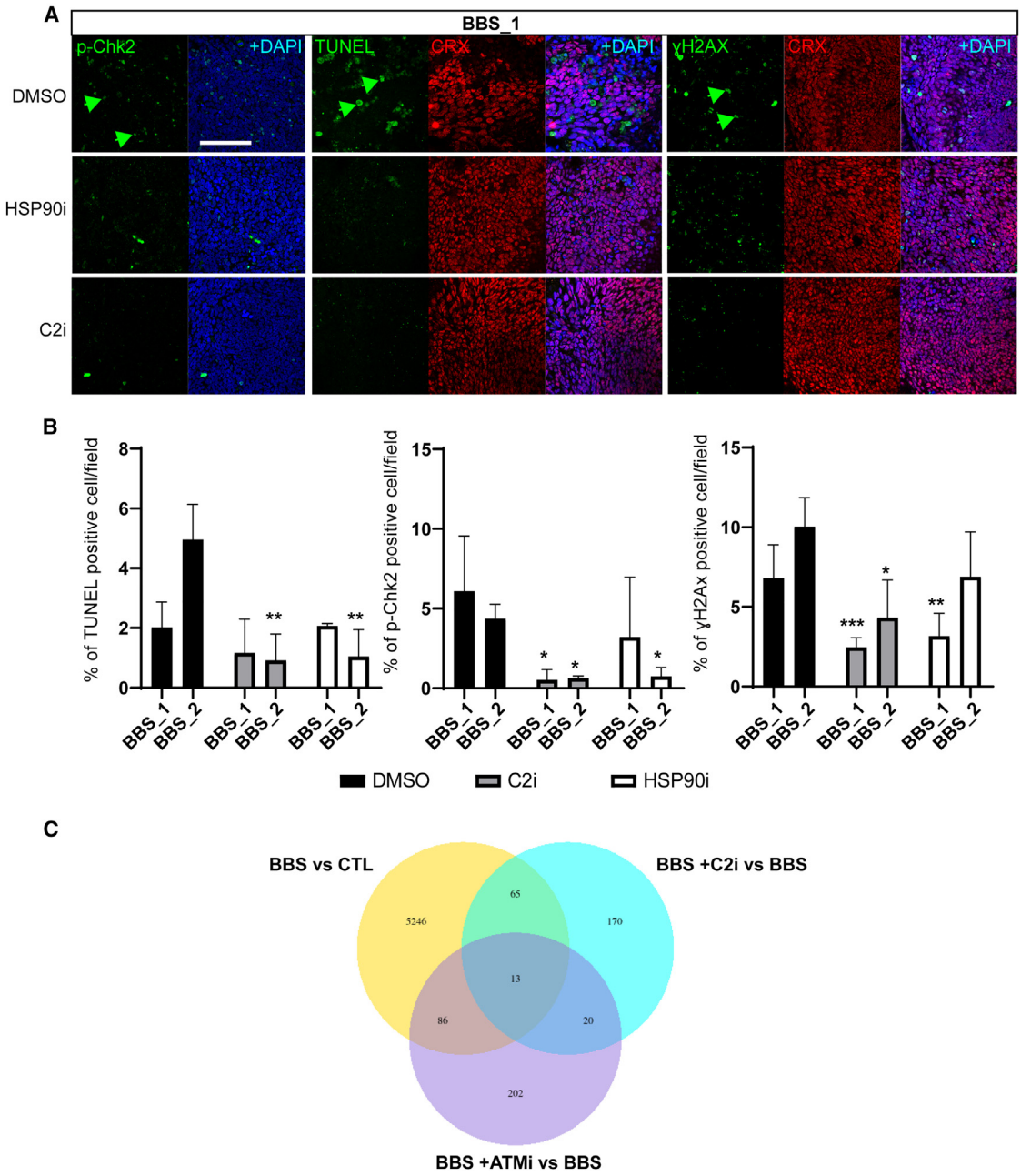

Figure 3. Inhibition of Chk2, ATM or HSP90 promotes BBS RPCs survival but does not restore the pathological transcriptome

(A) Representative confocal immunofluorescence images of BBS (BBS_1 case) RPCs at DIV15 treated for 5 days or not with HSP90i or C2i. Note the reduction in DDR proteins and cell death (TUNEL) in all treated conditions (green arrows). Scale bar: 50 μm.

(B) Quantification of CTL and BBS RPCs treated or not for 5 days with C2i or HSP90i. n = 4 replicates/group. All values are mean ± SEM.

(*) $p < 0.05$, (**) $p < 0.01$, (***) $p < 0.001$ by Student's unpaired t test.

(C) RNA-seq analysis of DIV15 RPCs from CTL and BBS groups, treated or not with C2i or ATMi. n = 2 replicates/group. N total = 16 samples.

experiments on BBS_1 and BBS_2 RPCs using C2i and HSP90i. C2i was found to be efficient at reducing cell death, p-Chk2 level, and γH2AX accumulation in RPCs from both BBS cases, with HSP90i performing generally less well (Figures 3A and 3B). Since Chk2 operates downstream of ATM in most DDR pathways, we investigated the efficiency of AZD1390, a blood-brain barrier permeable ATM inhibitor reported to present great potency and specificity at (10–100 μM).[56] BBS_1 and BBS_2 RPCs exposed to DMSO, C2i (10 μM), or ATMi (10 μM) were processed for RNA-seq analysis and compared to untreated CTL and BBS RPCs. This revealed that neither drug could substantially improve the deregulated transcriptome of BBS RPCs, as the

A

Up in BBS	Target	DMSO BBS/WT	C2i BBS Chk2i/WT	ATMi BBS ATMi/WT
	14-3-3 zeta/delta (Phospho-Thr232)	1,76	1,09	1,32
	ACC1 (Phospho-Ser80)	1,62	0,52	0,85
	AMPK1/AMPK2 (Phospho-Ser485/491)	1,38	1,04	1,05
	ATF2 (Phospho-Ser62/44)	1,56	0,81	1,15
	BAD (Phospho-Ser112)	1,44	0,87	1,14
	B-RAF (Phospho-Thr598)	1,74	0,97	1,27
BRCA1	BRCA1 (Phospho-Ser1524)	1,23	0,81	0,94
	CaMK2A (Phospho-Thr286)	1,26	1,00	0,96
Casp9	Caspase 9 (Phospho-Tyr153)	2,00	0,82	1,11
	Chk1 (Phospho-Ser286)	1,29	0,85	1,80
Chk1	Chk1 (Phospho-Ser317)	1,17	1,00	1,13
	Chk1 (Phospho-Ser345)	1,24	1,04	1,28
	Chk2 (Phospho-Thr383)	1,35	0,97	1,11
Chk2	Chk2 (Phospho-Ser516)	1,00	0,78	0,84
	Chk2 (Phospho-Thr68)	1,35	1,14	1,39
	Caveolin-1 (Phospho-Tyr14)	1,31	0,84	0,77
	c-Jun (Phospho-Tyr170)	1,49	0,97	1,14
CycE1	Cyclin E1 (Phospho-Thr77)	2,40	1,65	1,42
	EGFR (Phospho-Ser1070)	1,48	0,74	1,14
	Elk1 (Phospho-Ser383)	1,44	0,89	0,98
	Estrogen Receptor-alpha (Phospho-Ser106)	1,37	0,72	1,08
	FAK (Phospho-Ser910)	1,71	1,23	0,69
	FKHR (Phospho-Ser256)	1,55	1,14	1,23
	HDAC2 (Phospho-Ser394)	1,68	1,09	1,34
H2AX	Histone H2A.X (Phospho-Ser139)	1,71	1,15	1,36
HSP90B	HSP90B (Phospho-Ser254)	1,33	0,79	0,90
	IL-4R/CD124 (Phospho-Tyr497)	1,35	1,02	0,91
	IR (Phospho-Tyr1361)	2,02	1,58	1,42
	Kv1.3/KCNA3 (Phospho-Tyr135)	1,36	1,09	1,07
	LIMK1 (Phospho-Thr508)	1,86	1,26	1,36
	MEK1 (Phospho-Ser298)	2,40	1,13	1,64
p38 MAPK	p38 MAPK (Phospho-Tyr322)	2,68	1,52	1,72
	P90RSK (Phospho-Thr573)	3,23	2,33	1,19
	PKA CAT (Phospho-Thr197)	1,45	0,80	1,06
	PLC beta3 (Phospho-Ser1105)	1,36	0,63	0,79
	PLCG1 (Phospho-Tyr783)	1,44	1,09	1,03
	Rac1/cdc42 (Phospho-Ser71)	1,30	0,89	0,78
	Raf1 (Phospho-Ser338)	1,39	0,72	0,80
	Ras-GRF1 (Phospho-Ser916)	2,69	1,21	1,60
	S6 Ribosomal Protein (Phospho-Ser235)	1,35	0,94	0,98
	SHP-2 (Phospho-Tyr542)	2,67	1,94	1,94
	Src (Phospho-Tyr418)	2,58	1,62	1,35
	STAT5B (Phospho-Ser731)	1,81	1,06	1,23
	SYK (Phospho-Tyr348)	1,67	1,20	1,17
	Tau (Phospho-Thr181)	1,56	0,91	1,12
	Tyrosine Hydroxylase (Phospho-Ser31)	1,75	1,05	1,02
	VAV1 (Phospho-Tyr174)	2,01	1,35	1,49
	VEGFR2 (Phospho-Tyr1214)	1,34	0,84	1,04
	VEGFR2 (Phospho-Tyr951)	1,39	0,71	0,83

B

Down in BBS	Target	DMSO BBS/WT	C2i BBS Chk2i/WT	ATMi BBS ATMi/WT
	AKT1 (Phospho-Ser246)	0,56	0,80	0,97
	ATF2 (Phospho-Thr71/53)	0,77	1,10	0,95
	AurB (Phospho-Tyr12)	0,77	1,05	1,02
AurB	AurB (Phospho-Thr232)	0,67	1,07	0,92
BCL-2	BCL-2 (Phospho-Ser70)	0,57	0,91	0,82
	BTK (Phospho-Tyr223)	0,58	1,26	0,90
CDC25A	CDC25A (Phospho-Ser124)	0,79	1,21	1,13
CDC25B	CDC25B (Phospho-Ser353)	0,71	1,49	1,45
	Claudin 7 (Phospho-Tyr210)	0,72	0,95	0,89
	c-PLA2 (Phospho-Ser505)	0,77	1,32	1,26
	Crkii (Phospho-Tyr221)	0,80	1,23	1,20
CycD1	Cyclin D1 (Phospho-Thr286)	0,55	1,34	0,91
	EGFR (Phospho-Thr693)	0,67	1,00	1,15
	EPHB1/2 (Phospho-Tyr594/604)	0,65	0,88	0,87
	Epo-R (Phospho-Tyr368)	0,71	0,93	1,24
	FER (Phospho-Tyr402)	0,67	1,35	1,18
	GRK2 (Phospho-Ser29)	0,58	1,52	1,38
	GSK3 alpha (Phospho-Ser21)	0,69	1,83	1,79
	HER4/ErbB4 (Phospho-Tyr1284)	0,80	1,44	1,48
	HNF4 alpha (Phospho-Ser313)	0,79	1,31	1,12
	ICAM-1 (Phospho-Tyr512)	0,72	0,95	0,91
	IGF1R (Phospho-Tyr1161)	0,76	1,17	1,02
	Keratin 18 (Phospho-Ser52)	0,78	1,11	1,04
	LCK (Phospho-Ser59)	0,55	1,10	1,06
	M-CSF Receptor (Phospho-Tyr561)	0,69	1,14	1,04
	MEK1 (Phospho-Ser221)	0,33	1,01	0,73
	MEK2 (Phospho-Thr394)	0,74	1,22	1,37
	mTOR (Phospho-Thr2446)	0,70	0,84	1,01
	p27Kip1 (Phospho-Ser10)	0,61	1,28	0,96
p53	p53 (Phospho-Ser378)	0,67	1,20	0,97
	p53 (Phospho-Ser6)	0,76	1,00	0,94
	PDGFR alpha (Phospho-Tyr849)	0,72	1,38	0,96
	PDGFR beta (Phospho-Tyr740)	0,50	1,05	0,67
	PKC pan activation site (Phospho)	0,63	0,87	1,00
	PKC zeta (Phospho-Thr560)	0,77	0,96	0,97
	PKD2 (Phospho-Ser876)	0,61	0,75	0,83
	Smad2 (Phospho-Thr220)	0,72	1,12	1,19
	Smad3 (Phospho-Ser213)	0,71	1,02	0,93
	STAT4 (Phospho-Tyr693)	0,39	1,43	0,84

C

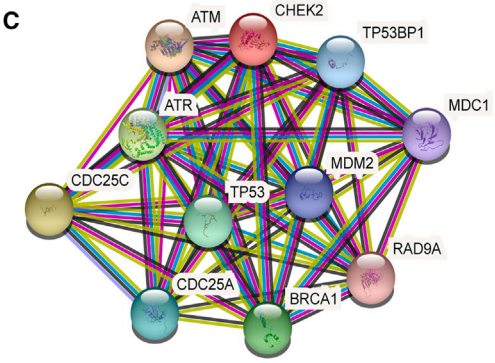

D

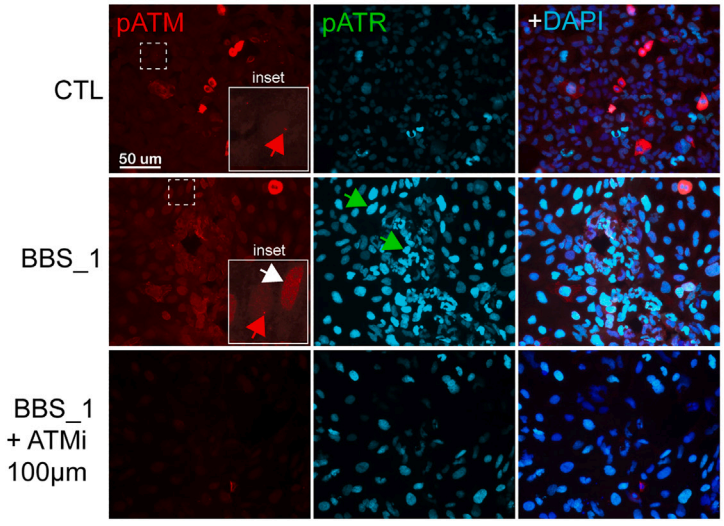

E

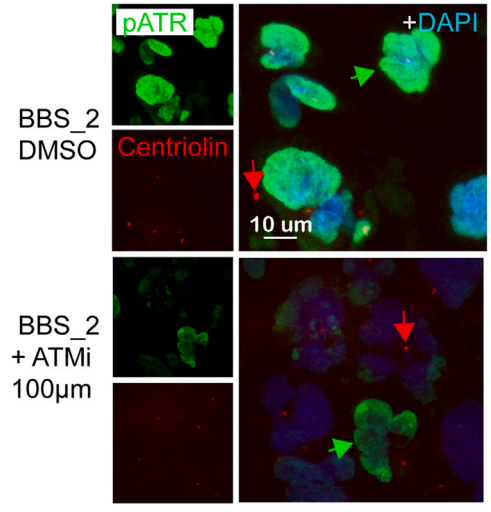

Figure 4. C2i or ATMi can restore the abnormal phospho-proteome in BBS RPCs

(A) Phospho-proteome analysis of DIV15 RPCs from CTL and BBS cases. RPCs were treated or not with DMSO, C2i, or ATMi and analyzed on micro glass-slides. *N* total = 4 micro-glass slides. Proteins with increased phosphorylation (target) in BBS are showed in red (DMSO). Green indicates reduced phosphorylation when compared to untreated CTL. White indicates equal phosphorylation when compared to untreated CTL.

(legend continued on next page)

profiles of the treated BBS were much more similar to untreated BBS than to CTL (Figure 3C).

C2i largely restores the abnormal phospho-proteome in BBS RPCs

Since the DDR and cell cycle are largely regulated by phosphorylation events, we performed a phospho-proteome analysis using CTL and BBS RPCs exposed to DMSO, C2i (10 μM) or ATMi (10 μM). Important differences in protein phosphorylation between control and BBS RPCs were found, with a higher proportion of hyper-phosphorylated proteins in BBS, including BRCA1, caspase-9, Chk1, Chk2, cyclin E1, H2AX, HSP90B, and p38MAPK (Figure 4A).[57] In turn, the phosphorylation of Aurora kinase B (AurkB), BCL-2, CDC25A, CDC25B, cyclin D1, and p53 was reduced in BBS (Figure 4B). AurkB phosphorylation at threonine 232 (Thr232) is the main activation site for AurkB autophosphorylation and phosphorylation of histone H3 (p-H3), leading to mitotic progression.[58] Notably, both C2i and ATMi greatly restored the abnormal BBS proteome for both hyper- and hypo-phosphorylated proteins, with C2i showing the best effect (Figures 4A and 4B). This DDR network was best represented using STRING analysis, showing interconnection with AurkB, CDC25 A/B, and cell death-pathways (Figure 4C). Because Chk1 and Chk2 are downstream of ATR and ATM, respectively, we investigated p-ATM and p-ATR. In RPCs, p-ATM localized to what appears to be centrosomes, but no obvious difference was observed between CTL and BBS (Figure 4D, red arrows in the insets). We also observed strong cytoplasmic labeling of p-ATM in cells ending mitosis (Figure 4D). In addition, a more widespread p-ATM signal resembling a generic DDR was observed only in BBS RPCs (Figure 4D, white arrow in the inset). While p-ATR labeling was generally weak in control RPCs, it was robust in in BBS RPCs, localizing to the nuclear envelope (Figures 4D and 4E).[59,60] Nuclear envelope deformation was also evident in in BBS RPCs, suggesting genomic instability (Figure 4E, green arrows). Double labeling with centriolin showed that p-ATR does not localize to centrosomes (Figure 4E). When used at a higher concentration, ATMi (100 μM) inhibited both p-ATM and p-ATR accumulation in BBS RPCs (Figures 4D and 4E), thus showing an off-target effect on ATR (see summary of results in Figure S4). This suggested that the DDR in BBS RPCs also involves ATM and ATR and that C2i can largely improve the abnormal BBS phospho-proteome.

C2i can improve tissue morphology and cone number in BBS retinal organoids

To test whether C2i could improve cone survival, we differentiated iPSCs into retinal sheets using the CI media.[36] At DIV60, neural rosettes were detached and put in suspension cultures, where they generated retinal organoids enriched in cone photoreceptors (Figure 5A).[61,62] Retinal sheets and then organoids were treated with C2i (10 μM) from DIV10 to DIV150, using a 5-day treatment and 2-day no treatment regimen as to reduce possible toxicity (Figure 5A). When compared with CTL at DIV27, we readily observed that BBS retinal sheets were less compact and had fewer neural rosettes, and that C2i treatment could ameliorate these parameters (Figure S5A). To investigate cone cell fate, retinal organoid's sections were analyzed using recoverin, OTX2, acetylated alpha tubulin, S-opsin, and M/L-opsin antibodies and PNA-FITC. When compared to CTL, BBS retinal organoids had tinner protruding inner/outer segments, and fewer M/L-opsin positive cells/section (Figure 5B and Di-iii, and S5B). Because of the high S-cone density owing to this specific differentiation protocol, it was not possible to quantify the number of S-opsin or recoverin positive cells. Notably, BBS retinal organoids also presented a disorganized retinal tissue, sometime showing holes within the presumptive inner neuroblastic layer (also referred as to the inner nuclear layer (INL)) (Figures 5B and 5C, red arrowheads). BBS organoids treated with C2i showed significantly more M/L-cones (Figures 5B and 5D), also sometime developing a visible OS (Figure 5B-insets). Disorganization of the BBS retinal tissue was also improved upon C2i treatment. When labeled with CRX and OTX2, both CTL and BBS organoids presented a presumptive ONL, which was generally thinner in BBS despite variations from sample to sample (Figures 5C-Div and S5B). ONL thickness was significantly improved by C2i in the BBS_2 case (Figure 5Div). C2i treatment in BBS retinal organoids thus improved tissue organization, cone OS maturation and M/L-cone number.

C2i reduces cell death and the DDR in BBS organoids

We used an activated caspase-3 antibody and the TUNEL assay to evaluate cell death. CTL organoids were nearly devoid of dying cells. In contrast, BBS organoids showed numerous dying cells in the presumptive ONL and INL, and cell death was significantly reduced by C2i treatment (Figures 6A and 6B). To measure the DDR, we first labeled the organoid's sections with CEP164, a centrosomal protein of the appendage involved in the DDR following ATM/ATR activation.[63,64] *CEP164* is mutated in BBS and nephronophthisis, and *Cep164*-null mice display retinal degeneration.[65,66] In both CTL and BBS organoids, CEP164 localization was enriched in the PNA-positive inner segment of cones, presumably at the BB, and CEP164 levels were visibly higher in BBS (Figure S6). We quantified the number of CEP164-positive foci and found that CTL and BBS retinal organoids had a similar number of CEP164 foci, yet with a slight increase observed in the BBS_1 case (Figure S6). This is consistent with previous work showing that the number of centrioles

(B) Proteins with reduced phosphorylation (target) in BBS are showed in green (DMSO).

(C) STRING analysis of the DDR network observed in *BBS10* RPCs using phospho-proteome and immunofluorescence analyses.

(D) Confocal immunofluorescence images of DIV15 CTL and BBS RPCs treated or not with ATMi. Note p-ATM localization at presumptive centrioles (red arrows-insets), and broad accumulation of p-ATR in BBS RPCs (green arrows). The white arrow in the inset (BBS case) depicts a classical DDR signal labeled by p-ATM. Scale bar: 50 μm.

(E) Confocal immunofluorescence images of DIV15 BBS RPCs treated with ATMi or not (DMSO). Deformation of the nuclear envelope in p-ATR positive BBS RPCs is indicated by the green arrows. The centriole is indicated by the red arrows. Note reduction of the p-ATR signal following ATMi treatment. Scale bar: 10 μm.

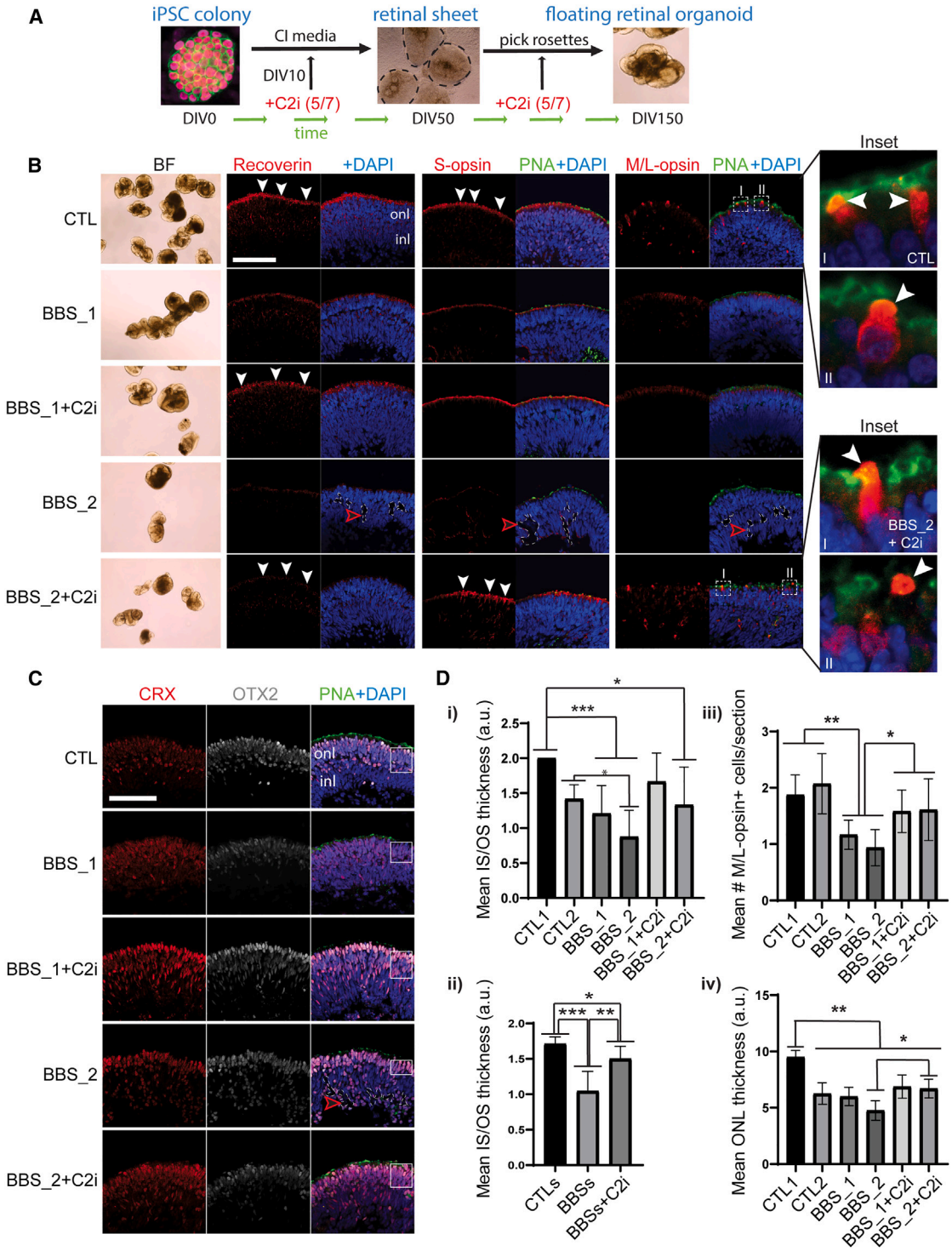

Figure 5. C2i promotes cone survival and OS maturation in BBS retinal organoids

(A) Schematic of the experimental setup. The iPSC colonies at near confluence were exposed to CI media and treated or not with C2i starting at DIV10. Neural rosettes from retinal sheets at DIV50 were manually picked and grown as suspension cultures to produce organoids. These were treated with C2i or not for an additional 100 days. C2i regiment was 5 days treatment and 2 days no-treatment.

(B) Bright field (BF) images of retinal organoids at DIV150 (left). Confocal immunofluorescence images (right) of CTL, BBS_1, and BBS_2 retinal organoid' sections treated with C2i or not. Note the formation of cone photoreceptor inner/outer segments (white arrowheads), with the outer segment most visible with the

(legend continued on next page)

is not affected BBS retinal precursors, in contrast with Meckel-Gruber syndrome retinal precursors which show supernumerary centrioles.[35] We next labeled the organoids with γH2AX, 53BP1 and p-ATM antibodies.[41] The DDR signal was robust in BBS_1 and BBS_2 retinal organoids and near absent in CTL (Figure 6A). However, we noticed that while the γH2AX signal was widespread in BBS retinal organoids, both 53BP1 and p-ATM preferentially localized to the upper most cells of the presumptive ONL (Figure 6A, white arrowheads). C2i treatment had no apparent effect on the γH2AX signal in BBS_1, and a small positive effect in BBS_2, but showed a robust positive effect on the 53BP1 and p-ATM signals (Figures 6A and 6B). The observed accumulation of DNA damage in BBS organoids may have resulted from the suboptimal C2i drug regiment (5/7) or from genomic instability of cells having bypassed and survived the G2/M checkpoint. Ki67 labeling revealed that many cells of the presumptive INL were in the cell cycle in CTL organoids. In BBS organoids, Ki67-positive cells were more frequent in the INL but were also visible in the ONL (Figure 6A). This suggested that C2i treatment cannot overcome DNA damage accumulation in BBS organoids but can inhibit the DDR and prevent cell death.

Cone precursors in BBS retinal organoids are arrested in metaphase/anaphase

AurkB is part of the chromosome passenger complex which controls proper chromosome alignment and segregation during mitosis.[67,68] While AurkA is present during G2/M and prophase, AurkB is predominant during metaphase, anaphase, and telophase of mitosis.[69] AurkB phosphorylates histone H3 at Serine 10 (p-H3) during metaphase and can also phosphorylate ATM to activate the spindle checkpoint.[70] To investigate mitosis in retinal organoids, they were labeled with AurkB, p-H3, and CHX10, which marks retinal progenitors of the INL during embryonic development and bipolar neurons after birth. Compared to CTL, BBS retinal organoids showed a normal INL thickness, as measured using CHX10, and the BBS INL was surprisingly thicker following C2i treatment (Figures 7A and S7A). This could be related to the previously reported upregulation of neural/retinal development and differentiation genes in BBS retinal precursors.[35] We observed that p-H3 positive cells were generally less abundant in BBS organoids when compared to CTL (Figures 7A and 7C). In turn, AurkB positive cells were generally more abundant in BBS organoids when compared to CTL, although substantial variation was observed within groups (Figures 7A and 7C). When measuring the number of AurkB/p-H3 double-positive cells, we found that they were generally located in the presumptive ONL and significantly more abundant in BBS organoids (Figures 7A and 7C). Morphological analysis also suggested that these AurkB/p-H3 double-positive cells were in metaphase/anaphase (Figure 7B arrowheads).[68] C2i treatment could significantly improve these phenotypes but only in the BBS_2 case (Figure 7C). With the limited information available on the BBS interactome, STRING analysis places BBS10 closest to HSP90A, which is linked to AURKB, H2AX, and BRCA1 (Figure S7B). In turn, centriolin (CNTRL) and CEP164 are closest to ATM, which is linked to ATR, Chk1, Chk2, and BRCA1 (Figure S7B). These results suggested that BBS cones and/or cone precursors arrest in the transition from metaphase to anaphase, and that C2i treatment releases this block, allowing mitotic progression and preventing cell death (see model in Figure 7D).

DISCUSSION

In this study, we observed that the initial production of cones in *Bbs10*$^{-/-}$ retinas is unaffected. However, at least starting from P10 onwards, *Bbs10*$^{-/-}$ mouse retinas show a DDR in the ONL, which persists and localizes to the nucleus and BB of surviving cones. At P10, the DDR correlates with the presence of TUNEL positive cells. Using directed differentiation of iPSCs, we showed that BBS RPCs display anomalies in sister chromatid segregation and activation of the mitotic spindle checkpoint. Chk2, ATM, and HSP90 inhibitors were able to improve the cell death and DDR phenotype of BBS RPCs. However, C2i was found to display the best effect, also improving the abnormal phospho-proteome. This led to the identification of the ATM/Chk2 and ATR/Chk1 pathways as central hubs in the BBS phenotype. Sustained treatment of BBS retinal organoids with C2i promoted cone photoreceptor survival and maturation, also improving retinal tissue organization and mitigating the DDR. Analyses of BBS organoids further suggests that cones or cone precursors are arrested in metaphase/anaphase, which can be partially overcome by C2i treatment.

Crosstalk between the DDR and the SAC is essential to maintain genomic stability. Although the fine-tuning mechanisms are still unresolved, it is well accepted that the ATM/Chk2 and ATR/Chk1 kinases are central mediators of this process.[33,71] We previously showed that BBS retinal precursors display hallmarks of genomic instability, including micronuclei, mitotic spindle anomalies and mitotic catastrophes.[35] Our present work further supports a non-canonical function of BBS10 at stabilizing centrosomes in RPCs. We observed that BBS RPCs display a DDR and undergo programmed cell death. In surviving post-mitotic

M/L-opsin staining (insets). Note the structural anomalies of the BBS retinal tissue (red arrowheads). Outer nuclear layer (onl), inner nuclear layer (inl). Scale bar: 100 μm.

(C) Confocal immunofluorescence images of CTL, BBS_1, and BBS_2 retinal organoid' sections treated with C2i or not. Note the structural anomalies of the BBS retinal tissue (red arrowhead). Boxes delineate the CRX and OTX2 positive onl, which was used to measure onl thickness. Outer nuclear layer (onl), inner nuclear layer (inl). Scale bar: 100 μm.

(D) Quantification of data from (B) and (C).

(Di and Dii) $n = 3$ sections/group of samples, with 3 measures/section.

(Di) is a representation of ungrouped samples.

(Dii) is a representation of grouped samples.

(Diii and Div) $n = 4$ sections/group of samples. All values are mean ± SEM.

(*) $p < 0.05$, (**) $p < 0.01$, and (***) $p < 0.001$ by Student's unpaired t test.

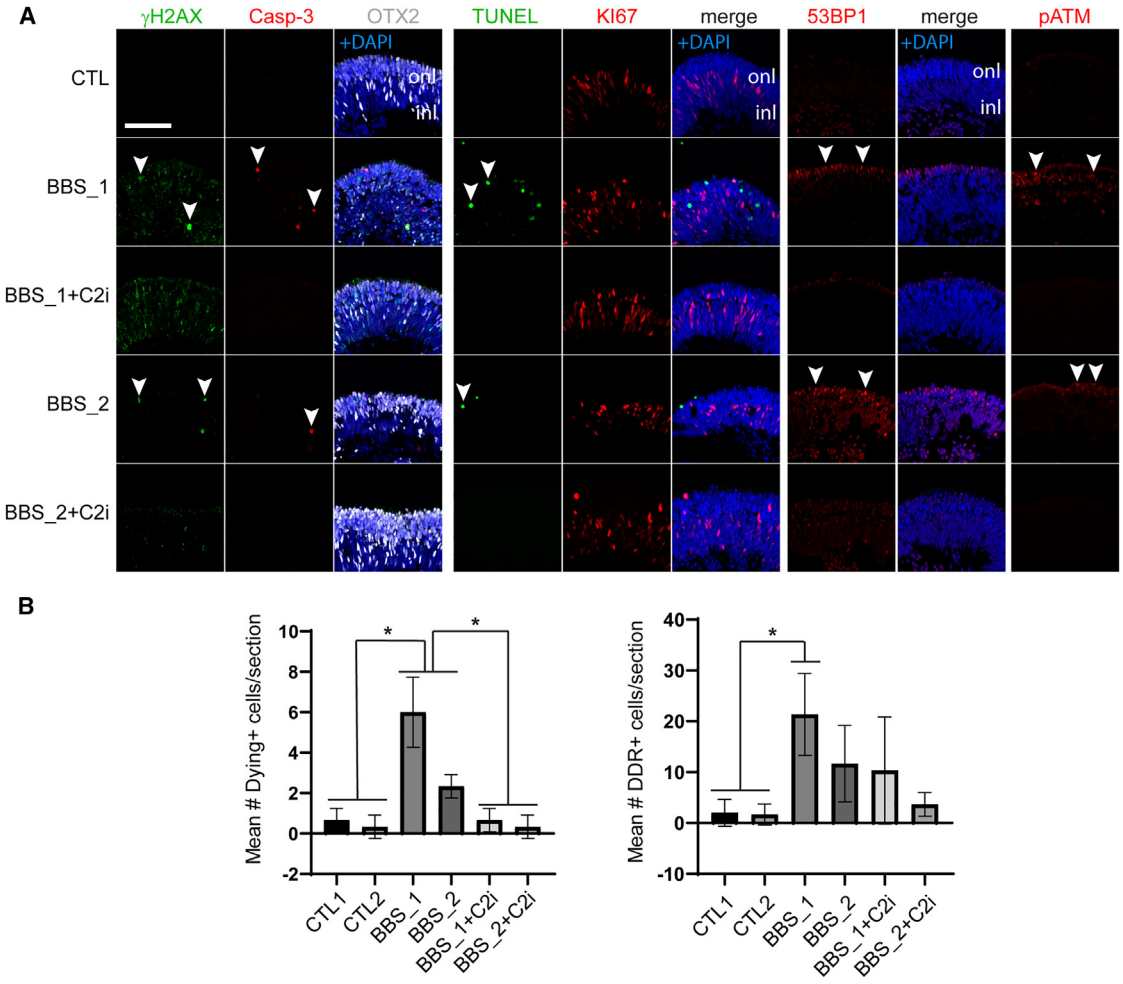

Figure 6. C2i mitigates cell death and the DDR in BBS retinal organoids

(A) Confocal immunofluorescence images of CTL, BBS_1, and BBS_2 retinal organoid' sections treated with C2i or not. Note the abundant DDR foci and TUNEL positive cells in BBS samples (white arrowheads). Outer nuclear layer (onl), inner nuclear layer (inl). Scale bar: 100 μm.

(B) Quantification of mean number of dying cells, as the sum of all cleaved caspase-3 and TUNEL positive cells/section. Quantification of mean number of DDR positive cells, as the sum of all γH2AX, 53BP1 and p-ATM positive cells/section. n = 9 sections/group. All values are mean ± SEM.

(*) $p < 0.05$ by Student's unpaired t test.

cones, this DDR persists at the nucleus and BB. We also showed that AurkB is hypo-phosphorylated at Thr232 in BBS RPCs, and that AurkB/p-H3 double-positive cones or cone precursors accumulate in metaphase/anaphase in BBS retinal organoids, thus when the SAC is ON to block mitotic progression.[33,72] RNA-seq analysis furthermore confirmed sister chromatid segregation anomalies in BBS RPCs. This is consistent with cell biology models suggesting that when the SAC is OFF, activated AurkB^{pThr232} represses PP1 kinetochore binding. When the SAC is ON, PP2A-B56 competes with AurkB activity to enhance PP1 kinetochore binding.[58,73] BBS10 belongs to the TCP-1 chaperonin family protein and is a probable molecular chaperone that may assist the folding of proteins upon ATP hydrolysis. As part of the BBS/CCT complex, BBS10 also plays a role in BBsome assembly, which is required for the formation/stability of the centrosome and BB.[15,17,19,20] *BBS10* mutations may thus result in centrosome instability, impeding proper association with microtubules during mitosis, leading to loss of tension with kinetochores and persistent SAC activation. By regulating BBsome assembly, BBS10 may also affect ciliary or centrosomal signaling, for instance of p-ATM which localizes to centrosomes. Notably, there is partial overlap between the machinery of the DDR and DNA replication, thus changes in expression of DDR proteins may also reflect effects of BBS10 on the cell cycle. Links between cilia, cell cycle, and DDR constitute an emerging field that requires further investigation to understand mechanistically. Others and we have previously showed that *Chk2* inactivation in *Bmi1*$^{-/-}$ mice improves growth and viability, and significantly delays cone photoreceptor degeneration.[74,75] In this model, photoreceptor cell death is predominant in cones, and occurs through activation of the Rip3 kinase, resulting in necroptosis.[75] While the *Bmi1*-mutation is unrelated to cilia or centrosome dysfunction, these findings point-out to a common pathological mechanism of photoreceptor

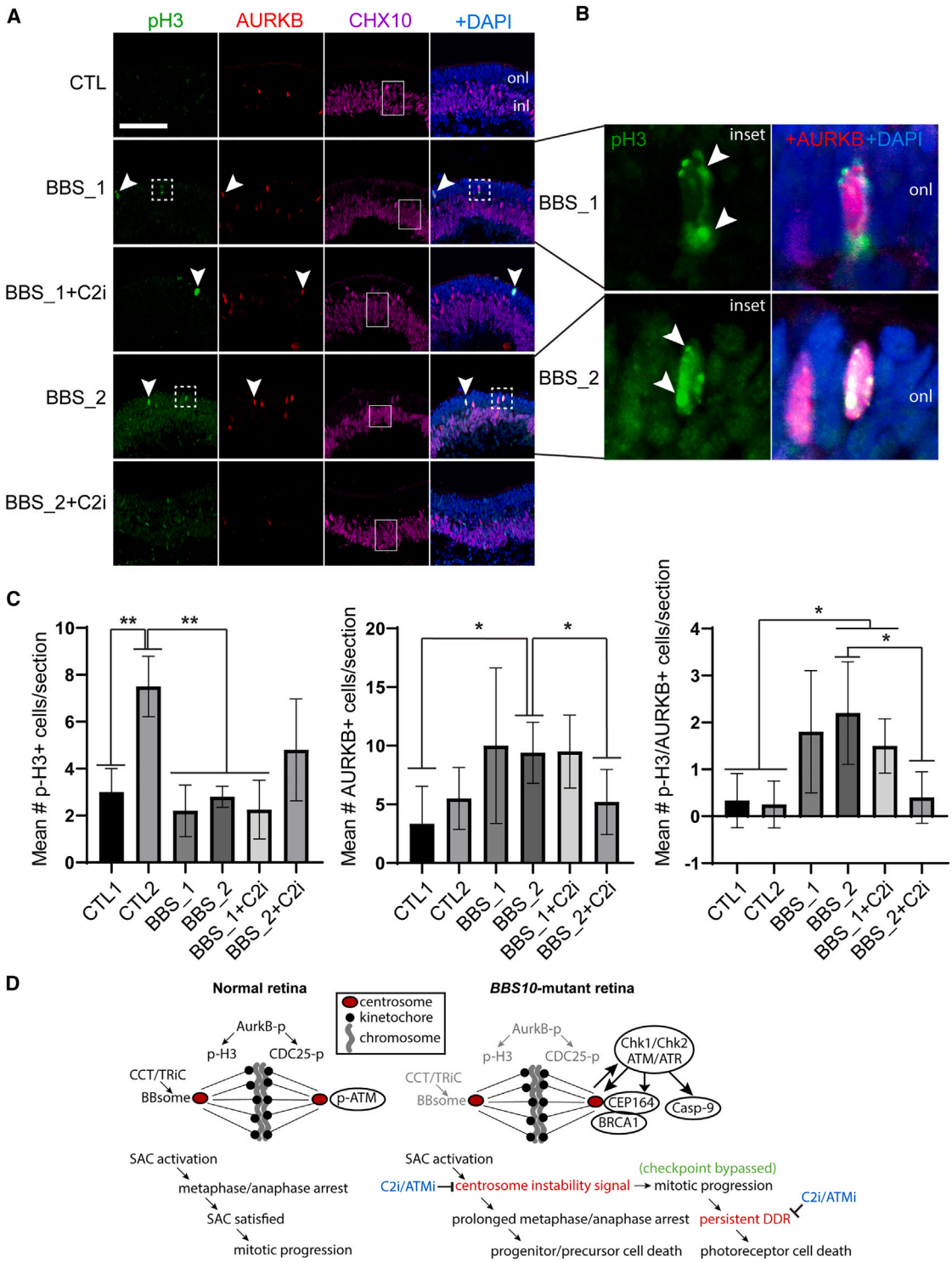

Figure 7. C2i improves BBS cone precursor metaphase/anaphase blockage

(A) Confocal immunofluorescence images of CTL, BBS_1, and BBS_2 retinal organoid' sections treated with C2i or not. Note the abundant p-H3/AurkB double-positive cells in BBS samples and located in the onl (white arrowheads). Boxed cells are showed as inset in (B). White boxes delineate Chx10-positive inl, which was used to quantified inl thickness. Outer nuclear layer (onl), inner nuclear layer (inl). Scale bar: 100 μm.

(B) Inset of cells boxed in (A). Note the p-H3/AurkB double-positive cells that are in metaphase/anaphase (white arrowheads).

(C) Quantification of results showed in (A) and (B). $n = 6$ sections/group. All values are mean ± SEM. (*) $p < 0.05$, (**) $p < 0.001$ by Student's unpaired t test.

(legend continued on next page)

degeneration involving genomic instability and cell cycle checkpoint activation.

In BBS patients with *BBS10* mutations and in *Bbs10*$^{-/-}$ mice, both cones and rods degenerate, yet cones appear to be affected earlier.[8,9,21] We have found that DDR-associated photoreceptor cell death in *Bbs10*$^{-/-}$ mice is predominant in cones. DDR-associated cell death was also observed in BBS RPCs and post-mitotic cones. However, because our BBS model lacks rods, we could not test if rod cell death in BBS organoids is DDR-dependent or not. Answering this question will be important for future application of our findings, since preventing rod degeneration in BBS patients would also represent a major milestone. Interspecies comparison suggests that the neonate human retina correspond to P10 retina in mice and rats.[76] Thus, and based on our findings in *Bbs10*$^{-/-}$ mice, any treatment aimed at preserving vision in BBS patients should start before the age of 2 years. The drug delivery method remains also a question since it is unknown if C2i (or ATMi) can cross the cornea and/or the blood-retinal barrier to reach the photoreceptor layer.

In conclusion, we revealed that a DDR linked to an ATM/Chk2 and ATR/Chk1-mediated mitotic spindle checkpoint is a central pathological mechanism of BBS RPCs. Persistent DDR at the nucleus and BB of cones having bypassed this checkpoint is predicted to also results in cell death (see working model in Figure 7D). We further showed that pharmaceutical inhibition of the Chk2 kinase can mitigates the DDR and cell death in BBS RPCs and promotes cone survival and OS maturation in BBS retinal organoids. This work may lend progress toward new treatments to prevent retinal degeneration in BBS patients.

Limitations of the study

The iPSC-based model of BBS retinal degeneration may not recapitulate events ongoing in affected patients, since evidence of a BBS embryonic, fetal, or neonatal retinal phenotype have not been documented. Yet, compensatory developmental mechanisms involving replacement of lost progenitor or precursor cells could mask observations made using the iPSC-based model system. The current protocol to induce retinal differentiation is biased to produce cone photoreceptors, thus precluding the study of BBS rods. Additional work is also needed to formally conclude that a DDR does not occur in *Bbs10*$^{-/-}$ mouse rods. We acknowledge that variations in neural differentiation efficiency, neural rosette formation, and retinal organoid development are inherent to all iPSC lines, and that having isogenic CTL and *BBS10*-KO iPSC lines would reduce variability and strengthen the findings. Only 2 biological replicates were used/sample for the RNA-seq analyses, impeding power for statistical analysis.

RESOURCE AVAILABILITY

Lead contact

Further information and requests for resources and reagents should be directed to and will be fulfilled by the lead contact, Gilbert Bernier. E-mail: gbernier.hmr@ssss.gouv.qc.ca. Tel: 514-252-3400 ext. 4648. Fax: 514-253-7626.

Materials availability

Raw data, cell lines, and reagents generated during this study are available upon reasonable request.

Data and code availability

- Data: RNA-seq data have been deposited at Gene Expression Omnibus (GEO) at Home - GEO DataSets - NCBI and are publicly available. Accession numbers are listed in the key resources table.
- Code: No custom code was generated in this manuscript.
- Any additional information required to reanalyze the data reported in this paper is available from the lead contact upon request.

ACKNOWLEDGMENTS

We are grateful to Dre Arlene Drack for the wt and *Bbs10*$^{-/-}$ mouse eyes. This work was supported in part by grants from the National Science and Engineering Research Council of Canada (NSERC), Stem Cell Network (Canada), and Maisonneuve-Rosemont Hospital Foundation. B.S.F. acknowledges support from NIH awards U01AI176460 and UH3TR003288. Graphical abstract has been created in BioRender: Barabino, A. (2024) https://BioRender.com/f17l082.

AUTHOR CONTRIBUTIONS

G.B., A.B., and R.H. conceived and designed the study; A.B. and R.H. performed the experiments; G.B., A.B., R.H., and A.K. analyzed the data; B.S.F. provided materials; G.B., A.B., R.H., and B.S.F. wrote the manuscript.

DECLARATION OF INTERESTS

G.B. is CEO, co-founder, and shareholder of StemAxonTM, a biotechnology company.

B.S.F. is CSO, co-founder and shareholder of Plurexa, a biotechnology company.

DECLARATION OF GENERATIVE AI AND AI-ASSISTED TECHNOLOGIES

No generative AI and AI assisted technologies have been used in this study.

STAR★METHODS

Detailed methods are provided in the online version of this paper and include the following:

- KEY RESOURCES TABLE
- EXPERIMENTAL MODEL AND STUDY PARTICIPANT DETAILS
  - Animals
  - Human cells
  - Cell cultures and retinal organoids
- METHOD DETAILS
  - RNA-seq analysis
  - Proteomic
  - Immunofluorescence
  - Antibodies
  - Terminal deoxynucleotidyl transferase dUTP nick end labeling assay

(D) Working model representing how the SAC and the DDR machinery are integrated to block cell cycle progression in BBS retinal cells. In normal cells, transient SAC activation ensures proper spindle assembly before mitotic progression. In BBS cells, a presumed "centrosome instability signal" owing to BBsome assembly defect results in an DDR triggering prolonged metaphase/anaphase arrest and progenitor cell death. Following successful mitotic progression, BBS photoreceptors present a persistent DDR, leading to neurodegeneration. Blocking the kinase activity of Chk2 or ATM in BBS cycling progenitors or post-mitotic photoreceptors mitigates the DDR, allowing cell survival.

SUPPLEMENTAL INFORMATION

Supplemental information can be found online at https://doi.org/10.1016/j.isci.2025.112130.

Received: June 18, 2024
Revised: September 5, 2024
Accepted: February 26, 2025
Published: March 1, 2025

REFERENCES

1. Hildebrandt, F., Benzing, T., and Katsanis, N. (2011). Ciliopathies. N. Engl. J. Med. *364*, 1533–1543. https://doi.org/10.1056/NEJMra1010172.
2. Reiter, J.F., and Leroux, M.R. (2017). Genes and molecular pathways underpinning ciliopathies. Nat. Rev. Mol. Cell Biol. *18*, 533–547. https://doi.org/10.1038/nrm.2017.60.
3. Derderian, C., Canales, G.I., and Reiter, J.F. (2023). Seriously cilia: A tiny organelle illuminates evolution, disease, and intercellular communication. Dev. Cell *58*, 1333–1349. https://doi.org/10.1016/j.devcel.2023.06.013.
4. Mill, P., Christensen, S.T., and Pedersen, L.B. (2023). Primary cilia as dynamic and diverse signalling hubs in development and disease. Nat. Rev. Genet. *24*, 421–441. https://doi.org/10.1038/s41576-023-00587-9.
5. Melluso, A., Secondulfo, F., Capolongo, G., Capasso, G., and Zacchia, M. (2023). Bardet-Biedl Syndrome: Current Perspectives and Clinical Outlook. Therapeut. Clin. Risk Manag. *19*, 115–132. https://doi.org/10.2147/TCRM.S338653.
6. Suspitsin, E.N., and Imyanitov, E.N. (2016). Bardet-Biedl Syndrome. Mol. Syndromol. *7*, 62–71. https://doi.org/10.1159/000445491.
7. Forsythe, E., and Beales, P.L. (2013). Bardet–Biedl syndrome. Eur. J. Hum. Genet. *21*, 8–13. https://doi.org/10.1038/ejhg.2012.115.
8. Grudzinska Pechhacker, M.K., Jacobson, S.G., Drack, A.V., Scipio, M.D., Strubbe, I., Pfeifer, W., Duncan, J.L., Dollfus, H., Goetz, N., Muller, J., et al. (2021). Comparative Natural History of Visual Function From Patients With Biallelic Variants in *BBS1* and *BBS10*. Investig. Ophthalmol. Vis. Sci. *62*, 26. https://doi.org/10.1167/iovs.62.15.26.
9. Gerth, C., Zawadzki, R.J., Werner, J.S., and Héon, E. (2008). Retinal morphology in patients with BBS1 and BBS10 related Bardet–Biedl Syndrome evaluated by Fourier-domain optical coherence tomography. Vis. Res. *48*, 392–399. https://doi.org/10.1016/j.visres.2007.08.024.
10. Lamb, T.D. (2016). Why rods and cones? Eye *30*, 179–185. https://doi.org/10.1038/eye.2015.236.
11. Bachmann-Gagescu, R., and Neuhauss, S.C. (2019). The photoreceptor cilium and its diseases. Curr. Opin. Genet. Dev. *56*, 22–33. https://doi.org/10.1016/j.gde.2019.05.004.
12. Chen, H.Y., Kelley, R.A., Li, T., and Swaroop, A. (2021). Primary cilia biogenesis and associated retinal ciliopathies. Semin. Cell Dev. Biol. *110*, 70–88. https://doi.org/10.1016/j.semcdb.2020.07.013.
13. Li, L., Anand, M., Rao, K.N., and Khanna, H. (2015). Cilia in photoreceptors. In Methods in Cell Biology, R. Basto and W.F. Marshall, eds. (Elsevier), pp. 75–92. https://doi.org/10.1016/bs.mcb.2014.12.005.
14. Wensel, T.G., Potter, V.L., Moye, A., Zhang, Z., and Robichaux, M.A. (2021). Structure and dynamics of photoreceptor sensory cilia. Pflügers Archiv *473*, 1517–1537. https://doi.org/10.1007/s00424-021-02564-9.
15. Seo, S., Baye, L.M., Schulz, N.P., Beck, J.S., Zhang, Q., Slusarski, D.C., and Sheffield, V.C. (2010). BBS6, BBS10, and BBS12 form a complex with CCT/TRiC family chaperonins and mediate BBSome assembly. Proc. Natl. Acad. Sci. USA *107*, 1488–1493. https://doi.org/10.1073/pnas.0910268107.
16. Wingfield, J.L., Lechtreck, K.-F., and Lorentzen, E. (2018). Trafficking of ciliary membrane proteins by the intraflagellar transport/BBSome machinery. Essays Biochem. *62*, 753–763. https://doi.org/10.1042/EBC20180030.
17. Tian, X., Zhao, H., and Zhou, J. (2023). Organization, functions, and mechanisms of the BBSome in development, ciliopathies, and beyond. Elife *12*, e87623. https://doi.org/10.7554/eLife.87623.
18. Zhang, Q., Yu, D., Seo, S., Stone, E.M., and Sheffield, V.C. (2012). Intrinsic Protein-Protein Interaction-mediated and Chaperonin-assisted Sequential Assembly of Stable Bardet-Biedl Syndrome Protein Complex, the BBSome. J. Biol. Chem. *287*, 20625–20635. https://doi.org/10.1074/jbc.M112.341487.
19. Álvarez-Satta, M., Castro-Sánchez, S., and Valverde, D. (2017). Bardet-Biedl Syndrome as a Chaperonopathy: Dissecting the Major Role of Chaperonin-Like BBS Proteins (BBS6-BBS10-BBS12). Front. Mol. Biosci. *4*, 55. https://doi.org/10.3389/fmolb.2017.00055.
20. Gupta, N., D'Acierno, M., Zona, E., Capasso, G., and Zacchia, M. (2022). Bardet–Biedl syndrome: The pleiotropic role of the chaperonin-like BBS6 , 10, and 12 proteins. Am. J. Med. Genet. C Semin. Med. Genet. *190*, 9–19. https://doi.org/10.1002/ajmg.c.31970.
21. Mayer, S.K., Thomas, J., Helms, M., Kothapalli, A., Cherascu, I., Salesevic, A., Stalter, E., Wang, K., Datta, P., Searby, C., et al. (2022). Progressive retinal degeneration of rods and cones in a Bardet-Biedl syndrome type 10 mouse model. Dis. Model. Mech. *15*, dmm049473. https://doi.org/10.1242/dmm.049473.
22. Delvallée, C., and Dollfus, H. (2023). Retinal Degeneration Animal Models in Bardet–Biedl Syndrome and Related Ciliopathies. Cold Spring Harb. Perspect. Med. *13*, a041303. https://doi.org/10.1101/cshperspect.a041303.
23. Datta, P., Allamargot, C., Hudson, J.S., Andersen, E.K., Bhattarai, S., Drack, A.V., Sheffield, V.C., and Seo, S. (2015). Accumulation of non-outer segment proteins in the outer segment underlies photoreceptor degeneration in Bardet–Biedl syndrome. Proc. Natl. Acad. Sci. USA *112*, E4400–E4409. https://doi.org/10.1073/pnas.1510111112.
24. Jiang, J., Promchan, K., Jiang, H., Awasthi, P., Marshall, H., Harned, A., and Natarajan, V. (2016). Depletion of BBS Protein LZTFL1 Affects Growth and Causes Retinal Degeneration in Mice. J. Genet. Genomics *43*, 381–391. https://doi.org/10.1016/j.jgg.2015.11.006.
25. Satir, P., and Christensen, S.T. (2007). Overview of Structure and Function of Mammalian Cilia. Annu. Rev. Physiol. *69*, 377–400. https://doi.org/10.1146/annurev.physiol.69.040705.141236.
26. Klena, N., and Pigino, G. (2022). Structural Biology of Cilia and Intraflagellar Transport. Annu. Rev. Cell Dev. Biol. *38*, 103–123. https://doi.org/10.1146/annurev-cellbio-120219-034238.
27. Hannaford, M.R., and Rusan, N.M. (2024). Positioning centrioles and centrosomes. J. Cell Biol. *223*, e202311140. https://doi.org/10.1083/jcb.202311140.
28. Gupta, G.D., Coyaud, É., Gonçalves, J., Mojarad, B.A., Liu, Y., Wu, Q., Gheiratmand, L., Comartin, D., Tkach, J.M., Cheung, S.W.T., et al. (2015). A Dynamic Protein Interaction Landscape of the Human Centrosome-Cilium Interface. Cell *163*, 1484–1499. https://doi.org/10.1016/j.cell.2015.10.065.
29. Ou, G., and Scholey, J.M. (2022). Motor Cooperation During Mitosis and Ciliogenesis. Annu. Rev. Cell Dev. Biol. *38*, 49–74. https://doi.org/10.1146/annurev-cellbio-121420-100107.
30. Dantas, T.J. (2020). Centrosomes and cilia: always at the center of the action. Commun. Biol. *3*, 785. https://doi.org/10.1038/s42003-020-01519-7.
31. Lara-Gonzalez, P., Westhorpe, F.G., and Taylor, S.S. (2012). The Spindle Assembly Checkpoint. Curr. Biol. *22*, R966–R980. https://doi.org/10.1016/j.cub.2012.10.006.
32. McAinsh, A.D., and Kops, G.J.P.L. (2023). Principles and dynamics of spindle assembly checkpoint signalling. Nat. Rev. Mol. Cell Biol. *24*, 543–559. https://doi.org/10.1038/s41580-023-00593-z.

33. Lawrence, K.S., and Engebrecht, J. (2015). The spindle assembly checkpoint: More than just keeping track of the spindle. Trends Cell Mol. Biol. *10*, 141–150.

34. Palou, R., Palou, G., and Quintana, D.G. (2017). A role for the spindle assembly checkpoint in the DNA damage response. Curr. Genet. *63*, 275–280. https://doi.org/10.1007/s00294-016-0634-y.

35. Barabino, A., Flamier, A., Hanna, R., Héon, E., Freedman, B.S., and Bernier, G. (2020). Deregulation of Neuro-Developmental Genes and Primary Cilium Cytoskeleton Anomalies in iPSC Retinal Sheets from Human Syndromic Ciliopathies. Stem Cell Rep. *14*, 357–373. https://doi.org/10.1016/j.stemcr.2020.02.005.

36. Zhou, S., Flamier, A., Abdouh, M., Tétreault, N., Barabino, A., Wadhwa, S., and Bernier, G. (2015). Differentiation of human embryonic stem cells into cone photoreceptors through simultaneous inhibition of BMP, TGFβ and Wnt signaling. Development *142*, 3294–3306. https://doi.org/10.1242/dev.125385.

37. Young, R.W. (1985). Cell differentiation in the retina of the mouse. Anat. Rec. *212*, 199–205. https://doi.org/10.1002/ar.1092120215.

38. Blackford, A.N., and Jackson, S.P. (2017). ATM, ATR, and DNA-PK: The Trinity at the Heart of the DNA Damage Response. Mol. Cell *66*, 801–817. https://doi.org/10.1016/j.molcel.2017.05.015.

39. Kinner, A., Wu, W., Staudt, C., and Iliakis, G. (2008). -H2AX in recognition and signaling of DNA double-strand breaks in the context of chromatin. Nucleic Acids Res. *36*, 5678–5694. https://doi.org/10.1093/nar/gkn550.

40. Rich, K.A., Zhan, Y., and Blanks, J.C. (1997). Migration and synaptogenesis of cone photoreceptors in the developing mouse retina. J. Comp. Neurol. *388*, 47–63.

41. Mirza-Aghazadeh-Attari, M., Mohammadzadeh, A., Yousefi, B., Mihanfar, A., Karimian, A., and Majidinia, M. (2019). 53BP1: A key player of DNA damage response with critical functions in cancer. DNA Repair *73*, 110–119. https://doi.org/10.1016/j.dnarep.2018.11.008.

42. Lei, T., Du, S., Peng, Z., and Chen, L. (2022). Multifaceted regulation and functions of 53BP1 in NHEJ-mediated DSB repair (Review). Int. J. Mol. Med. *50*, 90. https://doi.org/10.3892/ijmm.2022.5145.

43. Yim, H., Shin, S.-B., Woo, S.U., Lee, P.C.-W., and Erikson, R.L. (2017). Plk1-mediated stabilization of 53BP1 through USP7 regulates centrosome positioning to maintain bipolarity. Oncogene *36*, 966–978. https://doi.org/10.1038/onc.2016.263.

44. Zheng, Y., and Chen, S. (2024). Transcriptional precision in photoreceptor development and diseases – Lessons from 25 years of CRX research. Front. Cell. Neurosci. *18*, 1347436. https://doi.org/10.3389/fncel.2024.1347436.

45. Hoshino, A., Ratnapriya, R., Brooks, M.J., Chaitankar, V., Wilken, M.S., Zhang, C., Starostik, M.R., Gieser, L., La Torre, A., Nishio, M., et al. (2017). Molecular Anatomy of the Developing Human Retina. Dev. Cell *43*, 763–779. https://doi.org/10.1016/j.devcel.2017.10.029.

46. Glubrecht, D.D., Kim, J.H., Russell, L., Bamforth, J.S., and Godbout, R. (2009). Differential CRX and OTX2 expression in human retina and retinoblastoma. J. Neurochem. *111*, 250–263. https://doi.org/10.1111/j.1471-4159.2009.06322.x.

47. Sridhar, A., Hoshino, A., Finkbeiner, C.R., Chitsazan, A., Dai, L., Haugan, A.K., Eschenbacher, K.M., Jackson, D.L., Trapnell, C., Bermingham-McDonogh, O., et al. (2020). Single-Cell Transcriptomic Comparison of Human Fetal Retina, hPSC-Derived Retinal Organoids, and Long-Term Retinal Cultures. Cell Rep. *30*, 1644–1659. https://doi.org/10.1016/j.celrep.2020.01.007.

48. Dorgau, B., Collin, J., Rozanska, A., Zerti, D., Unsworth, A., Crosier, M., Hussain, R., Coxhead, J., Dhanaseelan, T., Patel, A., et al. (2024). Single-cell analyses reveal transient retinal progenitor cells in the ciliary margin of developing human retina. Nat. Commun. *15*, 3567. https://doi.org/10.1038/s41467-024-47933-x.

49. Patzke, S., Redick, S., Warsame, A., Murga-Zamalloa, C.A., Khanna, H., Doxsey, S., and Stokke, T. (2010). CSPP Is a Ciliary Protein Interacting with Nephrocystin 8 and Required for Cilia Formation. Mol. Biol. Cell *21*, 2555–2567. https://doi.org/10.1091/mbc.e09-06-0503.

50. Nuzhat, N., Van Schil, K., Liakopoulos, S., Bauwens, M., Rey, A.D., Käseberg, S., Jäger, M., Willer, J.R., Winter, J., Truong, H.M., et al. (2023). CEP162 deficiency causes human retinal degeneration and reveals a dual role in ciliogenesis and neurogenesis. J. Clin. Investig. *133*, e161156. https://doi.org/10.1172/JCI161156.

51. Smyczynska, U., Stanczak, M., Kuljanin, M., Włodarczyk, A., Stoczynska-Fidelus, E., Taha, J., Pawlik, B., Borowiec, M., Mancias, J.D., Mlynarski, W., et al. (2022). Proteomic and Transcriptomic Landscapes of Alström and Bardet–Biedl Syndromes. Genes *13*, 2370. https://doi.org/10.3390/genes13122370.

52. Fan, G., Sun, L., Meng, L., Hu, C., Wang, X., Shi, Z., Hu, C., Han, Y., Yang, Q., Cao, L., et al. (2021). The ATM and ATR kinases regulate centrosome clustering and tumor recurrence by targeting KIFC1 phosphorylation. Nat. Commun. *12*, 20. https://doi.org/10.1038/s41467-020-20208-x.

53. Brown, N., and Costanzo, V. (2009). An ATM and ATR dependent pathway targeting centrosome dependent spindle assembly. Cell Cycle *8*, 1997–2001. https://doi.org/10.4161/cc.8.13.8987.

54. Dodson, H., Bourke, E., Jeffers, L.J., Vagnarelli, P., Sonoda, E., Takeda, S., Earnshaw, W.C., Merdes, A., and Morrison, C. (2004). Centrosome amplification induced by DNA damage occurs during a prolonged G2 phase and involves ATM. EMBO J. *23*, 3864–3873. https://doi.org/10.1038/sj.emboj.7600393.

55. Smith, E., Dejsuphong, D., Balestrini, A., Hampel, M., Lenz, C., Takeda, S., Vindigni, A., and Costanzo, V. (2009). An ATM- and ATR-dependent checkpoint inactivates spindle assembly by targeting CEP63. Nat. Cell Biol. *11*, 278–285. https://doi.org/10.1038/ncb1835.

56. Durant, S.T., Zheng, L., Wang, Y., Chen, K., Zhang, L., Zhang, T., Yang, Z., Riches, L., Trinidad, A.G., Fok, J.H.L., et al. (2018). The brain-penetrant clinical ATM inhibitor AZD1390 radiosensitizes and improves survival of preclinical brain tumor models. Sci. Adv. *4*, eaat1719. https://doi.org/10.1126/sciadv.aat1719.

57. Matsuzawa, A., Kanno, S.I., Nakayama, M., Mochiduki, H., Wei, L., Shimaoka, T., Furukawa, Y., Kato, K., Shibata, S., Yasui, A., et al. (2014). The BRCA1/BARD1-Interacting Protein OLA1 Functions in Centrosome Regulation. Mol. Cell *53*, 101–114. https://doi.org/10.1016/j.molcel.2013.10.028.

58. Lee, H.-S., Min, S., Jung, Y.-E., Chae, S., Heo, J., Lee, J.-H., Kim, T., Kang, H.-C., Nakanish, M., Cha, S.-S., and Cho, H. (2021). Spatiotemporal coordination of the RSF1-PLK1-Aurora B cascade establishes mitotic signaling platforms. Nat. Commun. *12*, 5931. https://doi.org/10.1038/s41467-021-26220-z.

59. Kovacs, M.T., Vallette, M., Wiertsema, P., Dingli, F., Loew, D., Nader, G.P.D.F., Piel, M., and Ceccaldi, R. (2023). DNA damage induces nuclear envelope rupture through ATR-mediated phosphorylation of lamin A/C. Mol. Cell *83*, 3659–3668. https://doi.org/10.1016/j.molcel.2023.09.023.

60. Kumar, A., Mazzanti, M., Mistrik, M., Kosar, M., Beznoussenko, G.V., Mironov, A.A., Garrè, M., Parazzoli, D., Shivashankar, G.V., Scita, G., et al. (2014). ATR Mediates a Checkpoint at the Nuclear Envelope in Response to Mechanical Stress. Cell *158*, 633–646. https://doi.org/10.1016/j.cell.2014.05.046.

61. Barabino, A., Mellal, K., Hamam, R., Polosa, A., Griffith, M., Bouchard, J.-F., Kalevar, A., Hanna, R., and Bernier, G. (2023). Sub-retinal transplantation of human iPSC-derived retinal sheets: A promising approach for the treatment of macular degeneration. Preprint at bioRxiv. https://doi.org/10.1101/2023.10.19.

62. Barabino, A., Mellal, K., Hamam, R., Polosa, A., Griffith, M., Bouchard, J.-F., Kalevar, A., Hanna, R., and Bernier, G. (2024). Molecular characterization and sub-retinal transplantation of hypoimmunogenic human retinal sheets in a minipig model of severe photoreceptor degeneration. Development *151*, dev203071. https://doi.org/10.1242/dev.203071.

63. Chaki, M., Airik, R., Ghosh, A.K., Giles, R.H., Chen, R., Slaats, G.G., Wang, H., Hurd, T.W., Zhou, W., Cluckey, A., et al. (2012). Exome Capture

Reveals ZNF423 and CEP164 Mutations, Linking Renal Ciliopathies to DNA Damage Response Signaling. Cell *150*, 533–548. https://doi.org/10.1016/j.cell.2012.06.028.

64. Sivasubramaniam, S., Sun, X., Pan, Y.-R., Wang, S., and Lee, E.Y.-H.P. (2008). Cep164 is a mediator protein required for the maintenance of genomic stability through modulation of MDC1, RPA, and CHK1. Genes Dev. *22*, 587–600. https://doi.org/10.1101/gad.1627708.

65. Reed, M., Takemaru, K.-I., Ying, G., Frederick, J.M., and Baehr, W. (2022). Deletion of CEP164 in mouse photoreceptors post-ciliogenesis interrupts ciliary intraflagellar transport (IFT). PLoS Genet. *18*, e1010154. https://doi.org/10.1371/journal.pgen.1010154.

66. Maria, M., Lamers, I.J.C., Schmidts, M., Ajmal, M., Jaffar, S., Ullah, E., Mustafa, B., Ahmad, S., Nazmutdinova, K., Hoskins, B., et al. (2016). Genetic and clinical characterization of Pakistani families with Bardet-Biedl syndrome extends the genetic and phenotypic spectrum. Sci. Rep. *6*, 34764. https://doi.org/10.1038/srep34764.

67. Trivedi, P., and Stukenberg, P.T. (2020). A Condensed View of the Chromosome Passenger Complex. Trends Cell Biol. *30*, 676–687. https://doi.org/10.1016/j.tcb.2020.06.005.

68. Hadders, M.A., and Lens, S.M.A. (2022). Changing places: Chromosomal Passenger Complex relocation in early anaphase. Trends Cell Biol. *32*, 165–176. https://doi.org/10.1016/j.tcb.2021.09.008.

69. Willems, E., Dedobbeleer, M., Digregorio, M., Lombard, A., Lumapat, P.N., and Rogister, B. (2018). The functional diversity of Aurora kinases: a comprehensive review. Cell Div. *13*, 7. https://doi.org/10.1186/s13008-018-0040-6.

70. Yang, C., Tang, X., Guo, X., Niikura, Y., Kitagawa, K., Cui, K., Wong, S.T.C., Fu, L., and Xu, B. (2011). Aurora-B Mediated ATM Serine 1403 Phosphorylation Is Required for Mitotic ATM Activation and the Spindle Checkpoint. Mol. Cell *44*, 597–608. https://doi.org/10.1016/j.molcel.2011.09.016.

71. Luna-Maldonado, F., Andonegui-Elguera, M.A., Díaz-Chávez, J., and Herrera, L.A. (2021). Mitotic and DNA Damage Response Proteins: Maintaining the Genome Stability and Working for the Common Good. Front. Cell Dev. Biol. *9*, 700162. https://doi.org/10.3389/fcell.2021.700162.

72. Lawrence, K.S., Chau, T., and Engebrecht, J. (2015). DNA Damage Response and Spindle Assembly Checkpoint Function throughout the Cell Cycle to Ensure Genomic Integrity. PLoS Genet. *11*, e1005150. https://doi.org/10.1371/journal.pgen.1005150.

73. Nijenhuis, W., Vallardi, G., Teixeira, A., Kops, G.J.P.L., and Saurin, A.T. (2014). Negative feedback at kinetochores underlies a responsive spindle checkpoint signal. Nat. Cell Biol. *16*, 1257–1264. https://doi.org/10.1038/ncb3065.

74. Liu, J., Cao, L., Chen, J., Song, S., Lee, I.H., Quijano, C., Liu, H., Keyvanfar, K., Chen, H., Cao, L.-Y., et al. (2009). Bmi1 regulates mitochondrial function and the DNA damage response pathway. Nature *459*, 387–392. https://doi.org/10.1038/nature08040.

75. Barabino, A., Plamondon, V., Abdouh, M., Chatoo, W., Flamier, A., Hanna, R., Zhou, S., Motoyama, N., Hébert, M., Lavoie, J., et al. (2016). Retinal development anomalies and cone photoreceptors degeneration upon Bmi1 deficiency. Development *143*, 1571–1584. https://doi.org/10.1242/dev.125351.

76. Zeiss, C.J. (2021). Comparative Milestones in Rodent and Human Postnatal Central Nervous System Development. Toxicol. Pathol. *49*, 1368–1373. https://doi.org/10.1177/01926233211046933.

77. Love, M.I., Huber, W., and Anders, S. (2014). Moderated estimation of fold change and dispersion for RNA-seq data with DESeq2. Genome Biol. *15*, 550. https://doi.org/10.1186/s13059-014-0550-8.

78. Pearson, K. (1901). LIII. *On lines and planes of closest fit to systems of points in space*. London, Edinburgh Dublin Phil. Mag. J. Sci. *2*, 559–572. https://doi.org/10.1080/14786440109462720.

79. Gene Ontology Consortium; Aleksander, S.A., Balhoff, J., Carbon, S., Cherry, J.M., Drabkin, H.J., Ebert, D., Feuermann, M., Gaudet, P., and Harris, N.L. (2023). The Gene Ontology knowledgebase in 2023. Genetics *224*, iyad031. https://doi.org/10.1093/genetics/iyad031.

80. Ashburner, M., Ball, C.A., Blake, J.A., Botstein, D., Butler, H., Cherry, J.M., Davis, A.P., Dolinski, K., Dwight, S.S., Eppig, J.T., et al. (2000). Gene Ontology: tool for the unification of biology. Nat. Genet. *25*, 25–29. https://doi.org/10.1038/75556.

81. Subramanian, A., Tamayo, P., Mootha, V.K., Mukherjee, S., Ebert, B.L., Gillette, M.A., Paulovich, A., Pomeroy, S.L., Golub, T.R., Lander, E.S., and Mesirov, J.P. (2005). Gene set enrichment analysis: A knowledge-based approach for interpreting genome-wide expression profiles. Proc. Natl. Acad. Sci. USA *102*, 15545–15550. https://doi.org/10.1073/pnas.0506580102.

82. Fabregat, A., Korninger, F., Viteri, G., Sidiropoulos, K., Marin-Garcia, P., Ping, P., Wu, G., Stein, L., D'Eustachio, P., and Hermjakob, H. (2018). Reactome graph database: Efficient access to complex pathway data. PLoS Comput. Biol. *14*, e1005968. https://doi.org/10.1371/journal.pcbi.1005968.

83. Jassal, B., Matthews, L., Viteri, G., Gong, C., Lorente, P., Fabregat, A., Sidiropoulos, K., Cook, J., Gillespie, M., Haw, R., et al. (2020). The reactome pathway knowledgebase. Nucleic Acids Res. *48*, D498–D503. https://doi.org/10.1093/nar/gkz1031.

84. Griss, J., Viteri, G., Sidiropoulos, K., Nguyen, V., Fabregat, A., and Hermjakob, H. (2020). ReactomeGSA - Efficient Multi-Omics Comparative Pathway Analysis. Mol. Cell. Proteomics *19*, 2115–2125. https://doi.org/10.1074/mcp.TIR120.002155.

STAR★METHODS

KEY RESOURCES TABLE

REAGENT or RESOURCE	SOURCE	IDENTIFIER
Antibodies		
Sheep anti-Chx10	Exalpha Biologicals	X1180P
Rabbit anti-CORD2 (CRX)	GenTex	GTX124188
Rabbit anti-OTX2	Abcam	ab183951
Goat anti-OTX2	R&D Systems	AF1979
Rabbit anti-S-opsin	Invitrogen	OSO00006G
Rabbit anti-M/L-opsin	Chemicon	AB5405
Rabbit anti-Recoverin	Millipore	AB5585
Mouse anti-γH2AX	Millipore	05–636
Rabbit anti-53BP1	Novus	NB100-304
Rabbit anti-*p*-Chk2	Cell Signaling	2661
Mouse anti-*p*-ATM	Millipore	MAB3806-C
Rabbit anti-*p*-ATR	Millipore	SAB5701785
Anti-Ki67	Abcam	ab15580
Rabbit Anti-Histone H3 (phospho S10)	Abcam	ab5176
Anti-cleaved Caspase3	Cell Signaling	9661
Mouse Alpha acetyl tubulin	Santa Cruz	sc23950
Mouse Anti-AURKB	Novus	NBP2-50039
Mouse Anti-Centriolin	Santa Cruz	sc-365521
Anti-CEP164	Novus	NBP1-81445
PNA FITC	Vector Laboratories	FL-1071
Rhodamine Phalloidin	Invitrogen	R415
donkey AlexaFluor488-conjugated anti-mouse	Invitrogen	A-21202
donkey AlexaFluor488-conjugated anti-rabbit	Invitrogen	A-21206
donkey AlexaFluor488-conjugated anti-goat	Invitrogen	A-11055
donkey AlexaFluor568-conjugated anti-mouse	Invitrogen	A-10037
donkey AlexaFluor568-conjugated anti-rabbit	Invitrogen	A-10042
donkey AlexaFluor568-conjugated anti-goat	Invitrogen	A-11057
donkey AlexaFluor647-conjugated anti-mouse	Invitrogen	A-31571
donkey AlexaFluor647-conjugated anti-rabbit	Invitrogen	A-31573
donkey AlexaFluor647-conjugated anti-goat	Invitrogen	A-21447
goat AlexaFluor647-conjugated anti-mouse	Invitrogen	A-21235
goat AlexaFluor texas red-conjugated anti-rabbit	Invitrogen	T-2767
donkey AlexaFluor633-conjugated anti-sheep	Invitrogen	A-21100
Goat AlexaFluor594-conjugated anti-mouse IgM	Invitrogen	A-21044

(*Continued on next page*)

Continued

REAGENT or RESOURCE	SOURCE	IDENTIFIER
Chemicals, peptides, and recombinant proteins		
DMSO	Sigma-Aldrich	67-68-5
HSP90 inhibitor; Synonym: 4-(4-(2,3-Dihydro-1,4-benzodioxin-6-yl)-5-methyl-1H-pyrazol-3-yl)-6-ethylresorcinol	Sigma-Aldrich	171009-07-7
Chk2 inhibitor No1; Synonym: 5-(2-Amino-5-oxo-1,5-dihydroimidazol-4-ylidine)-3,4,5,10-2H-azepino[3,4-*b*]indol-1-one	Sigma-Aldrich	724708-21-8
Chk2 inhibitor No2; Synonym: 2-(4-(4-Chlorophenoxy)phenyl)-1H-benzimidazole-5-carboxamide	Sigma-Aldrich	516480-79-8
ATM inhibitor; Synonym: 2-(Morpholin-4-yl)-6-(thianthren-1-yl)-4H-pyran-4-one	Sigma-Aldrich	118502
p53 inhibitor/Pifithrin; Synonym: 2-(2-Imino-4,5,6,7-tetrahydrobenzothiazol-3-yl)-1-*p*-tolylethanone hydrobromide	Sigma-Aldrich	63208-82-2
ROCK inhibitor (Y-27632); Synonym: *trans*-4-[(1R)-1-aminoethyl]-N-4-pyridinyl-Cyclohexanecarboxamide, dihydrochloride	Cayman Chemical	10005583
Recombinant Human COCO Protein	R&D system	3047-CC-050
Recombinant Human IGF-1	Peprotech	100–11
Recombinant Human FGF basic	Peprotech	AF-100-18B
Heparin sodium salt from porcine intestinal mucosa	Sigma	H3149
Critical commercial assays		
Click-iT TUNEL Alexa Fluor Imaging Assay	Invitrogen	C10246
Phospho Explorer Antibody Array	from Full Moon BioSystems	PEX100
Deposited data		
RNAseq data	This paper	GEO accession: GSE269687
Experimental models: Cell lines		
iPSC Ctrl line 1	In house	Barabino et al.[35]
iPSC Ctrl line 2	Lab. C. Beauséjour	Barabino et al.[35]
BBS line 01 (Fibroblast cell line used to make in house iPSC)	Coriell	GM05948; Barabino et al.[35]
BBS line 02 (Fibroblast cell line used to make in house iPSC)	Coriell	GM05950; Barabino et al.[35]
Experimental models: Organisms/strains		
WT mice	Lab Dre Arlene Drack	Jackson Laboratory strain #014094
BBS10$^{-/-}$ mice	Lab Dre Arlene Drack	Generated from Jackson Laboratory strain #014094
Software and algorithms		
Fluoview software version 3.1		Olympus FluoView Resource Center: FluoView FV1000 Confocal Microscope Product Information
R software (R Core Team, 2013)		R: The R Foundation
GraphPad Prism 9 software		https://www.graphpad.com/
Phospho Explorer image quantification and analysis, data extraction, data organization and analysis	Full Moon BioSystems	Bioinformatic analysis service

EXPERIMENTAL MODEL AND STUDY PARTICIPANT DETAILS

Animals

Wild type and *Bbs10*$^{-/-}$ mouse eyes were generously obtained from Dre Arlene Drack.[21] This study was performed in strict accordance with the recommendations in the Guide for the Care and Use of Laboratory Animals of the National Institutes of Health. All the animals were handled according to approved Institutional Animal Care and Use Committee (IACUC) protocol #1041421 of the University of Iowa. The Bbs10 mouse model was acquired from the KOMP2 Center at the Jackson Laboratory, and it is now distributed through the Mutant Mouse Resource and Research Centers (MMRRC) as C57BL/6N-Bbs10tm1.1(KOMP)Vlcg/JMmucd. This mouse model was generated from the embryonic stem (ES) cell line Bbs10tm1(KOMP)Vlcg (VG13389A-A11, MMRRC). The C57BL6/NJ congenic version of the Sox2-Cre transgenic line (strain #014094, Jackson Laboratory) was used as a deleter line to generate the null allele. The characterization of this mouse model was described in detail in Mayer et al.[21] Animals were housed according to IACUC recommendations. Both male and female mice were used in this study. Animals were generated by crossing Bbs10$^{+/-}$ males with either Bbs10$^{+/-}$ or Bbs10$^{-/-}$ females. Mice were analyzed at three stages: P10, P45, and P60. Methods of euthanasia used were carbon dioxide inhalation followed by cervical dislocation. Humane endpoints were strictly observed, and every effort was made to minimize suffering.

Human cells

Human pluripotent stem cells were approved by the ''Comité de Surveillance de la Recherche sur les Cellules Souches'' of the CIHR and Maisonneuve-Rosemont Hospital Ethic Committee and used by following the Canadian Institute Health Research (CIHR) guidelines. All methods were carried out in accordance with relevant guidelines and regulations. Cell lines were authenticated, and the generation from dermal fibroblasts as well as the molecular characterization of CTL and BBS iPSC lines, including genetic characterization through WGA, was previously described in Barabino et al.[35] The BBS_01 case (Coriell accession number GM05948) was an affected 18-year-old male of white origin and carrying a homozygous c.271 duplication at the *BBS10* locus causing a frameshift stop in exon 2 (NCBI reference sequence NM_O24685.4). The BBS_02 case (Coriell accession number GM05950) was an affected 19-year-old male of white origin and carrying a compound heterozygous mutation (c.909_912 and c.687 deletions) also in exon 2 of the *BBS10* locus (NCBI reference sequence NM_O24685.4). iPSCs were tested for mycoplasma contamination using the LookOut Mycoplasma PCR Detection Kit (Sigma, MP0035).

Cell cultures and retinal organoids

Briefly, iPSCs were dissociated using TrypLE (Gibco Express Enzyme (1X), no phenol red, CAT# 12604013) and platted on growth factor reduced Matrigel (Corning #356231), in StemFit Basic04CT (Complete Type) Culture Medium (CAT# ASB04CT) with adding ROCK inhibitor (Y-27632; 10 μM, Cayman Chemical #10005583) for 24 h, then the media was changed without ROCK inhibitor. Upon confluency, cells were differentiated with CI media: DMEM-F12 medium (Invitrogen) containing 1% N2, 2% B27, 10 ng/mL IGF1 (PeproTech, Cat#100-11), and 5 ng/mL bFGF (PeproTech, Cat#AF-100-18B), Heparin (Sigma, Cat#H3149), and 30 ng/mL COCO (R&D System, Cat#3047-CC-050).[36] To generate retinal organoids, neural rosettes from DIV60 retinal sheet cultures were manually isolated with a 3mm biopsy punch and cultured in CI medium as suspension cultures in ultra-low adherence plates (Corning, CLS3473).[61,62]

METHOD DETAILS

RNA-seq analysis

Total RNA from 2 biological replicates for each genotype (CTL1, CTL2, BBS_1 and BBS_2 iPSC lines, $N = 8$ samples) and each treatment (BBS_1 + C2i, BBS_2 + C2i, BBS1+ATMi, BBS_2+ATMi, $N = 8$ samples) was extracted using the standard procedure of Qiagen columns and assayed for RNA integrity. cDNA was prepared according to the manufacturer's instructions (NEB library) and sequenced using the Illumina platform. Base-calling and feature count were done using HISAT2 on the HG19 genome. For differential expression analysis, DESeq2[77] was used on R program (Team, R. C. The R Project for Statistical Computing. http://www.R-Project.Org/1–12 (2013) at https://www.r-project.org/). Global gene expression was visualized using volcano plots and heatmaps for top genes. Samples were clustered and visualized in a 2D space using PCA.[78] For functional analysis, the differentially expressed genes, or a subset of those genes, were analyzed using Gene Ontology (GO), Gene Set Enrichment Analysis (GSEA) and Reactome.[79–84]

Proteomic

Phospho Explorer Antibody Array containing 1318 antibodies (with 99% reactivity against human epitopes) was obtained from Full Moon BioSystems (Cat. No. PEX100) and used accordingly to manufacturer instructions. Array image quantification and analysis, including data extraction, data organization and analysis of the array images was obtained through the company service.

Immunofluorescence

Cells and organoids were fixed for 1 h at room temperature in 4% paraformaldehyde (PFA)/3% sucrose in PBS, pH 7.4. Organoids were washed three times in PBS, cryoprotected in PBS/30% sucrose, and frozen in CRYOMATRIX embedding medium (CEM)

(Thermo Shandon, Pittsburgh, PA) or in Tissue-Tek optimum cutting temperature (O.C.T.) compound (Sakura Finetek, USA). Cells and organoids were permeabilized with Triton X-100 for 10 min. Unspecific antigen blocking was performed using 2% BSA in PBST for 30 min. Slides were incubated with the primary antibody overnight at 4°C in a humidified chamber. Secondary antibodies were incubated for 1h at room temperature. After incubation with the secondary antibody, slides were washed, counterstained with DAPI and mounted using VECTASHIELD Antifade Mounting Medium (VECTASHIELD, H-1000-10) and No. 1.5H coverslips. Pictures were taken using a confocal microscopy system (Olympus). Confocal microscopy analyses were performed using 60x objectives with an IX81 confocal microscope (Olympus, Richmond Hill, Canada), and images were obtained with Fluoview software version 3.1 (Olympus). For quantification in *Bbs10*$^{-/-}$ mouse retinas, images were taken from the ventro-nasal part of the retina, and near the optic nerve head.

Antibodies

Primary antibodies used in this study are sheep anti-Chx10 (1:250, Exalpha Biologicals, X1180P), rabbit anti-CORD2 (CRX) (1:300, GenTex, GTX124188), rabbit anti-OTX2 (1:300, Abcam, ab183951), goat anti-OTX2 (1:500, R&D Systems, AF1979), rabbit anti-S-opsin (1:200, Invitrogen, OSO00006G), rabbit anti-M/L-opsin (1:100, Chemicon, AB5405), rabbit anti-Recoverin (1:1000, Millipore, AB5585), mouse anti-γH2AX (1:250, Millipore, 05–636), rabbit anti-53BP1 (1:250, Novus, NB100-304), rabbit anti-*p*-Chk2 (1:250, Cell Signaling, 2661), mouse anti-*p*-ATM (1:250, Millipore, MAB3806-C), rabbit anti-*p*-ATR (1:250, Millipore, SAB5701785), anti-Ki67 (1:500, Abcam, ab15580), rabbit anti-Histone H3 (phospho S10) (1:500, Abcam, ab5176), anti-cleaved Caspase3 (1:1000, Cell Signaling, 9661), mouse alpha acetyl tubulin (1:300, Santa Cruz, sc23950), mouse anti-AURKB (1:300, Novus, NBP2-50039), mouse anti-Centriolin (1:300, Santa Cruz, sc-365521), anti-CEP164 (1:300, Novus, NBP1-81445), PNA FITC (1:200, Vector Laboratories, FL-1071), and rhodamine phalloidin (1:200, Invitrogen, R415). Secondary antibodies used in this study are donkey AlexaFluor488-conjugated anti-mouse (1:1000, Invitrogen, A-21202), donkey AlexaFluor488-conjugated anti-rabbit (1:1000, Invitrogen, A-21206), donkey AlexaFluor488-conjugated anti-goat (1:1000, Invitrogen, A-11055), donkey AlexaFluor568-conjugated anti-mouse (1:1000, Invitrogen, A-10037), donkey AlexaFluor568-conjugated anti-rabbit (1:1000, Invitrogen, A-10042), donkey AlexaFluor568-conjugated anti-goat (1:1000, Invitrogen, A-11057), donkey AlexaFluor647-conjugated anti-mouse (1:1000, Invitrogen, A-31571), donkey AlexaFluor647-conjugated anti-rabbit (1:1000, Invitrogen, A-31573), donkey AlexaFluor647-conjugated anti-goat (1:1000, Invitrogen, A-21447), goat AlexaFluor647-conjugated anti-mouse (1:1000, Invitrogen, A-21235), goat AlexaFluor Texas Red-conjugated anti-rabbit (1:1000, Invitrogen, T-2767), donkey AlexaFluor633-conjugated anti-sheep (1:1000, Invitrogen, A-21100), and goat AlexaFluor594-conjugated anti-mouse IgM (1:1000, Invitrogen, A-21044).

Terminal deoxynucleotidyl transferase dUTP nick end labeling assay

For detection of apoptotic cell death, cells were fixed in 4% PFA. Terminal deoxynucleotidyl transferase dUTP nick end labeling (TUNEL) staining was performed using a Click-iT TUNEL Alexa Fluor Imaging Assay (Invitrogen, C10246) following the manufacturer's instructions.

Chemical treatment of cell culture

In this study, specific chemical inhibitors were utilized to treat the cell cultures. DMSO (CAS 67-68-5) served as the control treatment. The following inhibitors were employed: HSP90 inhibitor (CAS 171009-07-7), Chk2 inhibitor No. 1 (CAS 724708-21-8), Chk2 inhibitor No. 2 (CAS 516480-79-8), ATM inhibitor (CAS 118502), and p53 inhibitor/Pifithrin (CAS 63208-82-2). All chemicals were obtained from Sigma-Aldrich.

Treatment concentrations of 1 μM, 10 μM, and 100 μM were used. Dissociated cell cultures were treated with these inhibitors for a duration of 5 days.

For long-term treatments, retinal sheets and organoids were subjected to a regimen using Chk2 inhibitor No. 2 (C2i) at a concentration of 10 μM, from day *in vitro* (DIV) 10 to DIV 150. The treatment protocol consisted of a 5-day treatment followed by a 2-day no-treatment period to mitigate potential toxicity.

QUANTIFICATION AND STATISTICAL ANALYSIS

Statistical analysis

Statistical analyses were performed using GraphPad Prism 9 software or R software (R Core Team, 2013). Prior to performing statistical tests, the assumptions of normality and equal variances were assessed. If these assumptions were met, a Student's t test for unpaired samples was used to compare two groups. For multiple comparisons among more than two groups, a one-way analysis of variance (ANOVA) followed by Dunnett's test was conducted. The assumption of normality of residuals and homogeneity of variances across groups were verified before applying ANOVA. All values in the figures are expressed as mean ± standard error of the mean (SEM). The criterion for statistical significance (P-value) is indicated in each figure legend as follows: $^{*}p < 0.05$; $^{**}p < 0.01$; $^{***}p < 0.001$.